Toxoplasma membrane inositol phospholipid binding protein TgREMIND is essential for secretory organelle function and host infection

Rodrigue Houngue, Lamba Omar Sangaré, Tchilabalo Dilezitoko Alayi, Aissatou Dieng, Tristan Bitard-Feildel, Claire Boulogne, Christian Slomianny, Cynthia Menonve Atindehou, Lucie Ayi Fanou, Yetrib Hathout, et al.

Cell Reports

Article

Toxoplasma membrane inositol phospholipid binding protein *Tg*REMIND is essential for secretory organelle function and host infection

Graphical abstract

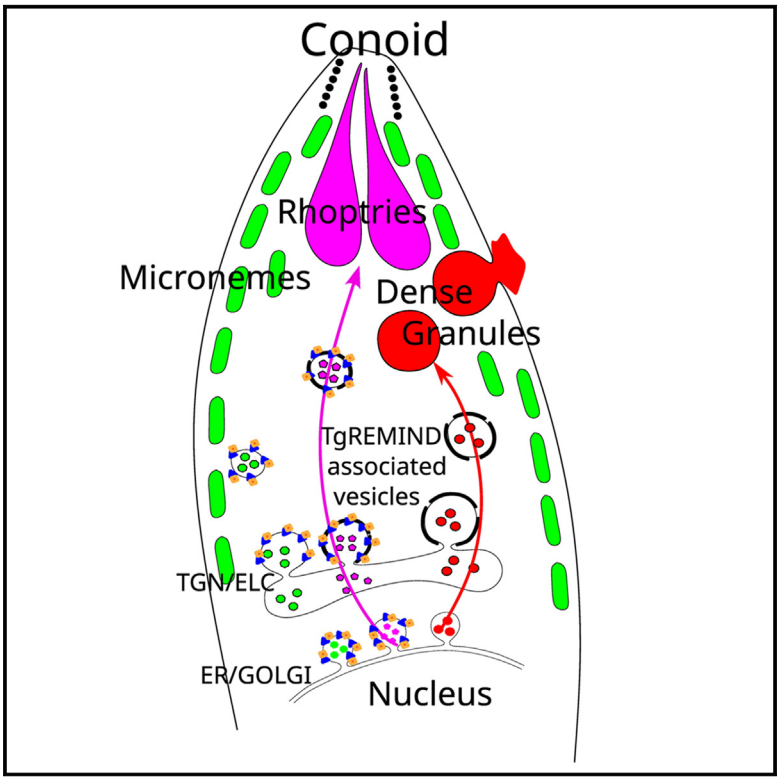

Authors

Rodrigue Houngue, Lamba Omar Sangaré, Tchilabalo Dilezitoko Alayi, ..., Yetrib Hathout, Isabelle Callebaut, Stanislas Tomavo

Correspondence

stanislas.tomavo@gmail.com

In brief

In this study, Houngue et al. describe an essential role for the uncharacterized protein named *Tg*REMIND, for regulator of membrane-interacting domain, in the biogenesis of rhoptries and dense granules, two secretory organelles that contain virulence factors released during and after *Toxoplasma* cell invasion.

Highlights

- *Tg*REMIND is a membrane-associated protein binding to PIP2 lipids
- Both F-BAR domain and REMIND of *Tg*REMIND are required for PIP2 binding
- *Tg*REMIND is essential for the biogenesis of rhoptries and dense granules in *Toxoplasma*
- Inactivation of *Tg*REMIND abolished *Toxoplasma* host cell invasion and dissemination

Houngue et al., 2024, Cell Reports *43*, 113601
January 23, 2024
https://doi.org/10.1016/j.celrep.2023.113601

CellPress

Cell Reports

CellPress
OPEN ACCESS

Article

Toxoplasma membrane inositol phospholipid binding protein *Tg*REMIND is essential for secretory organelle function and host infection

Rodrigue Houngue,[1,8] Lamba Omar Sangaré,[2,8] Tchilabalo Dilezitoko Alayi,[3,8] Aissatou Dieng,[1] Tristan Bitard-Feildel,[4] Claire Boulogne,[1,5] Christian Slomianny,[6] Cynthia Menonve Atindehou,[7] Lucie Ayi Fanou,[7] Yetrib Hathout,[3] Isabelle Callebaut,[4] and Stanislas Tomavo[1,9,*]

[1]Université Paris Saclay, CNRS UMR 9198-CEA, Institute for Integrative Biology of the Cell (I2BC), 91190 Gif sur Yvette, France
[2]Department of Biology, Texas A&M University, College Station, TX 77843, USA
[3]Department of Pharmaceutical Science, School of Pharmacy and Pharmaceutical Sciences, Binghamton University−SUNY, Johnson City, NY 13790, USA
[4]Sorbonne Université, Muséum National d'Histoire Naturelle, UMR CNRS 7590, Institut de Minéralogie, de Physique des Matériaux et de Cosmochimie, IMPMC, 75005 Paris, France
[5]Plateforme Imagerie-Gif, Institut de Biologie Intégrative de la Cellule (I2BC), 91190 Gif sur Yvette, France
[6]University of Lille, Laboratory of Cell Physiology, INSERM U 1003, 59655 Villeneuve d'Ascq, France
[7]Université d'Abomey Calavi, Laboratoire de Biochimie et de Biologie Moléculaire, Faculté des Sciences et Technologies, Cotonou, Bénin
[8]These authors contributed equally
[9]Lead contact
*Correspondence: stanislas.tomavo@gmail.com
https://doi.org/10.1016/j.celrep.2023.113601

SUMMARY

Apicomplexan parasites possess specialized secretory organelles called rhoptries, micronemes, and dense granules that play a vital role in host infection. In this study, we demonstrate that *Tg*REMIND, a protein found in *Toxoplasma gondii*, is necessary for the biogenesis of rhoptries and dense granules. *Tg*REMIND contains a Fes-CIP4 homology-Bin/Amphiphysin/Rvs (F-BAR) domain, which binds to membrane phospholipids, as well as a novel uncharacterized domain that we have named REMIND (regulator of membrane-interacting domain). Both the F-BAR domain and the REMIND are crucial for *Tg*REMIND functions. When *Tg*REMIND is depleted, there is a significant decrease in the abundance of dense granules and abnormal transparency of rhoptries, leading to a reduction in protein secretion from these organelles. The absence of *Tg*REMIND inhibits host invasion and parasite dissemination, demonstrating that *Tg*REMIND is essential for the proper function of critical secretory organelles required for successful infection by *Toxoplasma*.

INTRODUCTION

Toxoplasma gondii is an obligate intracellular eukaryotic parasite of the phylum Apicomplexa, which includes the deadly human malaria pathogen *Plasmodium falciparum*. Toxoplasmosis is principally dangerous to fetuses of primoinfected pregnant women and individuals with compromised immune systems.[1,2] Infection by *T. gondii* is lifelong and incurable, leaving chronically infected people susceptible to reactivated disease, including severe ocular disorders and vision loss.[3,4] After entry into the host cell, *T. gondii* establishes its permissive replication niche, named the parasitophorous vacuole (PV), which is demarcated from the host cytoplasm by a membrane (PVM).[5] To develop inside the host cell, apicomplexan parasites possess unique morphological features constituting the phylum's hallmark.[6,7] Among these features is the remarkable apical complex composed of the polar ring, the conoid, and lineage-specific secretory organelles called rhoptries and micronemes that play an essential role in apicomplexan parasite pathogenesis.[8–13] In addition, a third secretory organelle called a dense granule releases GRA proteins that are involved in the formation of the PV, in which the parasites replicate intracellularly, and in several other functions, such as transfer of small molecules from the host cytoplasm into the PV.[5,14] The molecular mechanisms of and functions performed by the rhoptry (ROP), microneme (MIC), and dense granule (GRA) proteins during host cell attachment, invasion, and survival are described in more detail elsewhere.[10,11,15–18] However, the underlying mechanisms involved in the biogenesis of these organelles and their maintenance throughout the parasite replication cycle are not well understood. The secretory organelles are synthesized *de novo* during the replication and budding of the daughter parasites formed within the mother.[19] However, it has been described that a significant number of micronemes are also recycled from the mother parasites to the newly formed daughters.[20] The transport of ROP and MIC proteins depends on their appropriate timing of expression, which suggests that their intracellular trafficking is directly associated with secretory organelle biogenesis.[16,21] However, more information is needed

about how the parasite-specific factors that supply these secretory organelles are differentially sorted and transported in a timely, coordinated, and regulated fashion. We reported that forming these vital secretory organelles requires the *T. gondii* sortilin-like receptor *Tg*SORTLR, also named *Tg*SORT.[22,23] The N-terminal and luminal ectodomain of the receptor binds ROP and MIC proteins. In contrast, the cytosolic tail binds to the *Tg*Vps35-retromer complex to recruit partners to enable anterograde and retrograde receptor transport.[24] Here, we describe a new parasite-specific protein, *Tg*REMIND, which contains a highly conserved Fes-CIP4 homology-Bin/Amphiphysin/Rvs (F-BAR) domain at the N terminus and a novel uncharacterized REMIND (for regulator of membrane-interacting domain) at the C terminus. The presence of both F-BAR domain and REMIND in this protein, which is therefore named *Tg*REMIND, is necessary for its activities in the parasites. Conditional targeted ablation demonstrates that mutants devoid of *Tg*REMIND lose dense granules and typical opaque rhoptries, leading to severe inhibition of host cell invasion. Our findings illustrate the key role of *Tg*REMIND, a lipid-binding protein, in the formation and functions of secretory organelles required for host infection and parasite dissemination.

RESULTS

Identification of molecular features associated with functions of *Tg*REMIND

In this study, we aimed to uncover any additional functions of the retromer complex[24] beyond recycling *T. gondii* sortilin (*Tg*SORT). We conducted experiments involving knockin (KI) parasites of *Tg*Vps35 with a hemagglutinin (HA) tag in the conditional iKO-*Tg*SORT mutant.[22] We observed that, in the absence of *Tg*SORT, a fraction of the *Tg*Vps35 diffused into the parasite's cytoplasm. However, most of the *Tg*Vps35 remained correctly located in the endosomal-like compartment (ELC), indicating that the retromer may play a role in recycling other cargoes.[24] To investigate this further, we performed comparative co-immunoprecipitation (coIP) with *Tg*Vps35 in the presence and absence of *Tg*SORT using total protein extracts from anhydrotetracycline (ATc)-treated or untreated KI-*Tg*Vps35-HA/iKO-*Tg*SORT parasites and anti-HA antibodies coupled to agarose beads. The two coIP eluates were subjected to mass spectrometry analysis followed by a semi-quantitative label-free method to identify partners binding to the *Tg*Vps35-retromer complex in the presence or absence of *Tg*SORT (Figure S1A). *T. gondii* hypothetical protein 25 (*Tg*HP25) was significantly more abundant in the coIP without *Tg*SORT vs. its presence (Figure S1B). Next, we used computational tools (see STAR Methods) to identify *Tg*HP25 as a new *T. gondii* regulator containing an F-BAR domain (InterPro IPR027267), which is known to interact with membranes.[25,26] Therefore, *Tg*HP25 was named *Tg*REMIND. *Tg*REMIND comprises two foldable domains, separated by a large, disordered region (Figure S2A), and a stretch of several serine residues at the end of the C terminus of the protein (Figure S2B). The first foldable domain (aa 79–369) shares significant similarities with the F-BAR domains of known 3D structures, such as the tyrosine-protein kinase Fes/Fps (PDB: 4DYL), formin-binding protein 17 (PDB: 2EFL), and septation protein Imp2 (PDB: 5C1F) F-BAR domains. The second foldable domain (aa 507–825; Figure S2A), which we named REMIND, does not share apparent similarities with sequences of known 3D structures, but its middle part (aa 588–749) matches the Pfam SET binding factor 2 (SBF2) profile (PF12335). It is worth noting that the F-BAR domain is present in several homologs of *Tg*REMIND in different apicomplexan parasites (Figure S3). To the best of our knowledge, none of these *Tg*REMIND homologs containing F-BAR domains have been characterized in the other parasites. A search of the UniProt reference proteomes using PSI-BLAST identified significant similarities between the sequence of the C-terminal region of REMIND and that of proteins of alveolata and Oomycetes species, where it is also associated with an N-terminal F-BAR domain (Figures 1A and S4). The REMIND C-terminal region was also detected in other eukaryotic proteins, associated with other domains such as TBC (Tre-2, BUB2p, and Cdc16p) characteristic of Rab GTPase-activating proteins (GAPs). It is also linked to the upstream u-DENN (differentially expressed in normal and neoplastic cells), core c-DENN, and downstream d-DENN domains (Rab guanine nucleotide exchange factors [GEFs]) in human MADD as well as in human MTMR5 and MTMR13, both members of the myotubularin-related protein family (Figures 1A and S4).

*Tg*REMIND predominantly resides in the cytoplasm and in the vicinity of rhoptries and dense granules

We produced specific mouse polyclonal antibodies against recombinant GST-tagged full-length *Tg*REMIND ($aa_{1–976}$), the F-BAR domain ($aa_{1–386}$), and REMIND ($aa_{387–976}$), respectively. These three polyclonal antibodies recognize a single band around 140 kDa (Figure S5A), which was exclusively expressed in parasites and not in uninfected human foreskin fibroblasts (HFFs) (Figure 1B). However, this protein size is larger than the predicted molecular mass of *Tg*REMIND (TGGT1_259720, see www.toxodb.org), estimated at 100 kDa. We also appended an encoded c-Myc tag to *Tg*REMIND using a KI strategy that ensures steady-state levels of epitope-tagged protein expression via homologous promoters.[27] Again, the anti-cMyc antibodies recognized a band around 140 kDa (Figure S5B). This difference in molecular size could be due to the chemical nature and behavior of the amino acids of *Tg*REMIND or the presence of several stretches of three to five serine residues at the C terminus of the protein (Figure S2B), suggesting multiple possible post-translational modifications. Confocal imaging using anti-*Tg*REMIND (Figure 1C) and anti-cMyc (Figure S5C, top left) antibodies revealed labeling of the cytoplasm of *T. gondii* with a stronger signal at the apical region above the nucleus. This strong fluorescence near the nucleus appeared close to *Tg*SORTLR and *Tg*Vps35 (Figure S5C). *Tg*REMIND signal also appeared near the pre-organelle and ELC markers pro-ROP4 and pro-MIC5 (Figure S5D). Based on the locations of different compartments and organelles of *T. gondii* shown by the schematic representation in Figure 1D, *Tg*REMIND partially co-distributed with ROP1 and ROP5 (Figures 1E and 1F) but also with ROP7 (Figure S5E). Quantifying these confocal images showed that 15% ± 3% of ROP1 and 20% ± 5% of ROP5 proteins co-distributed with *Tg*REMIND (Figure 1I). In addition, we found that 17% ± 3% of GRA5 co-distributed with *Tg*REMIND (Figures 1G and 1I). In contrast,

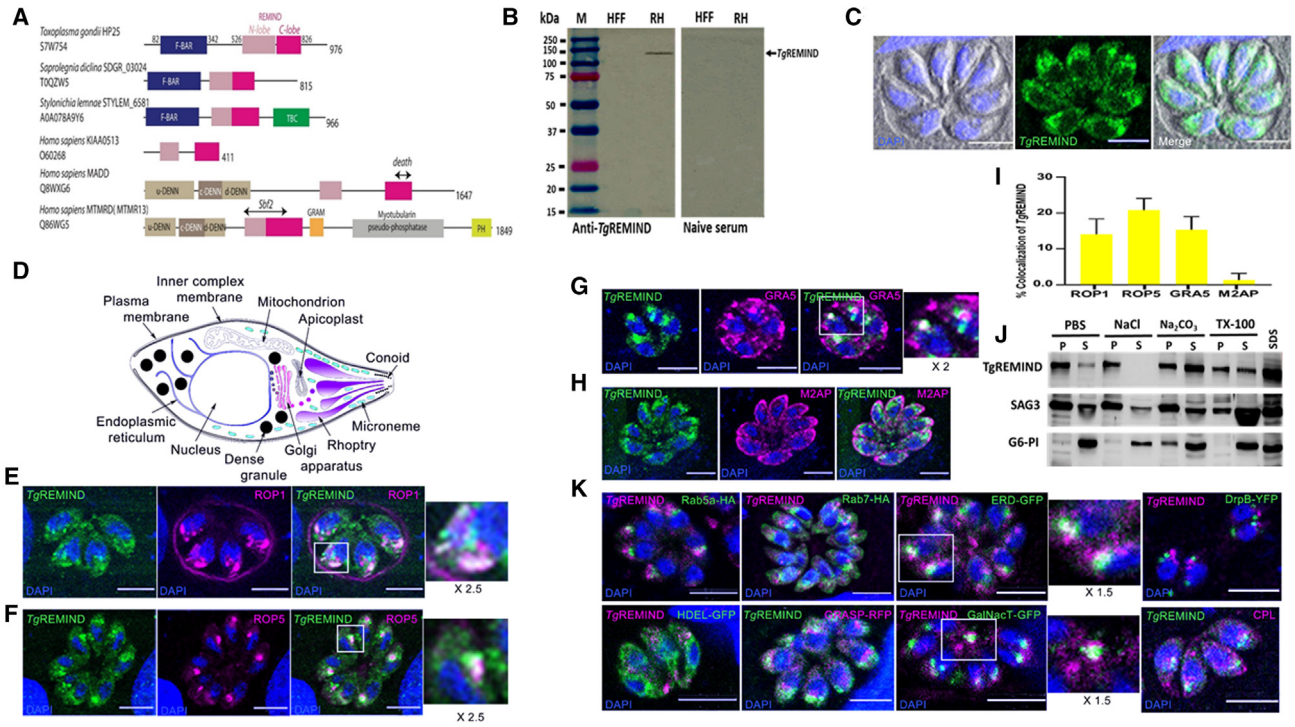

Figure 1. *Tg*REMIND is a membrane-bound F-BAR domain protein present in different subcellular compartments

(A) Domain architecture of representative members of the REMIND family.

(B) Immunoblots probed with mouse polyclonal anti-*Tg*REMIND antibodies using *T. gondii* (RH strain). Human foreskin fibroblasts (HFF) and naive sera showed no protein bands, as expected.

(C) Localization of *Tg*REMIND using anti-*Tg*REMIND antibodies and confocal microscopy.

(D) Schematic representation of *T. gondii*.

(E–G) *Tg*REMIND partially co-localizes with the ROP1 (E) and ROP5 (F) proteins. (G) *Tg*REMIND also partially co-localizes with the GRA5 protein.

(H) *Tg*REMIND shows no co-localization with the micronemal protein M2AP.

(I) Quantification of *Tg*REMIND co-distribution with ROP1, ROP5, GRA5, and M2AP. Bars represent n = 3 independent experiments ± standard deviation (SD).

(J) Cell fractionation on wild-type *T. gondii* parasites and western blots using *Tg*REMIND, GPI-anchored surface antigen 3, and the glycolytic enzyme glucose 6-phosphate isomerase (G6-PI).

(K) Confocal images of intracellular parasites transiently transfected with plasmids expressing markers of different compartments and organelles and probed with anti-*Tg*REMIND antibodies. Scale bar, 5 μm.

there was no co-distribution between the microneme M2AP protein and *Tg*REMIND (Figures 1H and 1I). Together with the presence of the F-BAR domain, these data suggest a close vicinity of *Tg*REMIND and different intracellular membrane compartments in *T. gondii*, including the ELC, where the ROP and MIC proteins traffic and mature before reaching apical secretory organelles.

*Tg*REMIND interacts with cellular membrane components and secretory organelles

To corroborate the location of *Tg*REMIND with its biochemical properties, we lysed extracellular parasites with PBS alone or PBS containing either detergent or other chaotropic agents and separated the insoluble proteins (P) from the soluble (S) fraction. Under these conditions, *Tg*REMIND was insoluble in PBS alone and in PBS containing 0.5 M NaCl but partially soluble by detergent extraction (2% Triton X-100) and much more when extracted by sodium carbonate (Na_2CO_3) (Figure 1J). In contrast, detergent (Triton X-100) extracted the positive control membrane glycosyl phosphoribosyl inositol (GPI)-anchored surface antigen 3 (GPI-SAG3), whereas the cytosolic glycolytic enzyme glucose 6-phosphate isomerase (G6-PI) was soluble in PBS, as expected (Figure 1J). Sodium carbonate extraction is a canonical way to distinguish integral membrane proteins from other moderately hydrophobic membrane-associated proteins,[28] suggesting that a significant amount of *Tg*REMIND binds to subcellular membranes that are present in the cytoplasm of *T. gondii*. Furthermore, using other subcellular markers of *T. gondii*, we observed a weak co-localization with the post-Golgi compartment (ERD-GFP and N-acetylgalactosaminyl transferase [GalNAc-T]) and late ELC such as Rab7-HA (Figure 1K), indicating that *Tg*REMIND is present in distinct subcellular compartments of the parasite simultaneously. However, no co-distribution was found with the endoplasmic reticulum (ER; HDEL-GFP), the marker of acidified organelles (CPL), the Golgi (GRASP-RFP), or the dynamin-related compartment (DRpB-YFP),[29] suggesting that *Tg*REMIND does not interact with these later compartments (Figure 1K).

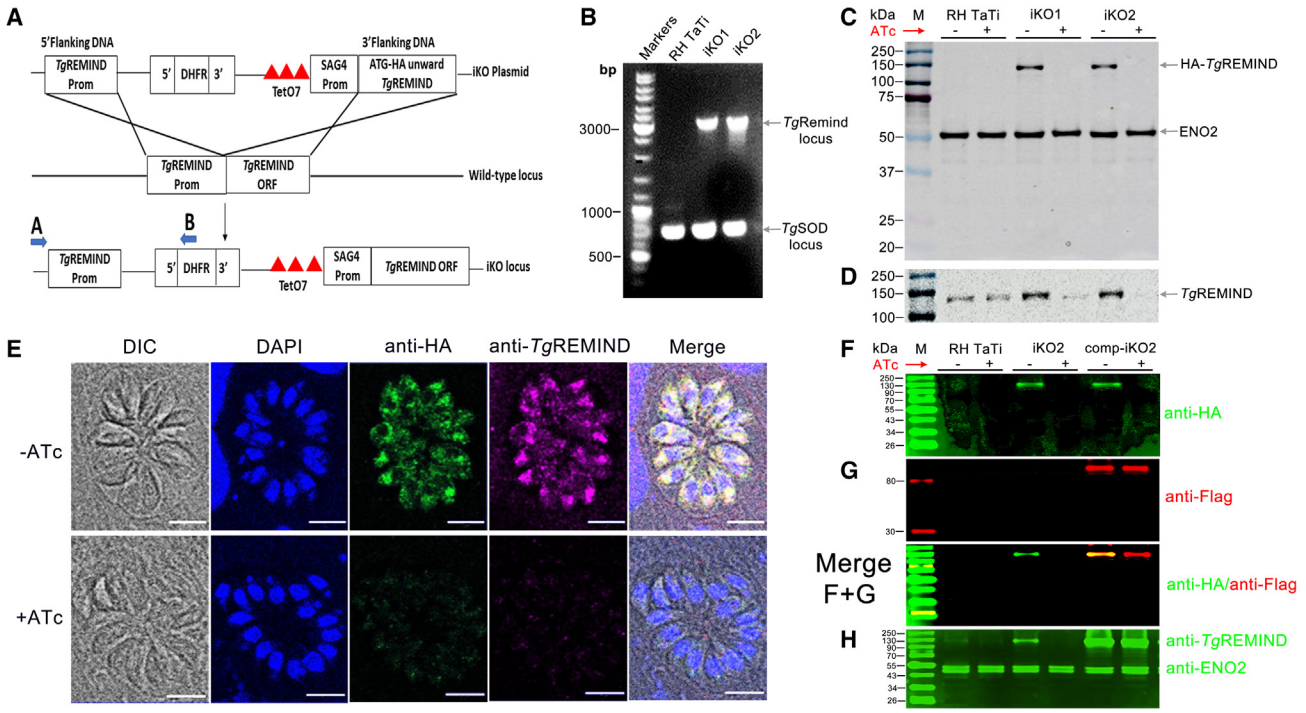

Figure 2. Conditional ablation of *Tg*REMIND gene and complementation

(A) Schematic of the approach used for the conditional ablation of the *Tg*REMIND gene.

(B) PCR analysis using the primers A and B (see blue arrows in A) confirms the conditional targeted ablation of *Tg*REMIND. *T. gondii* superoxide dismutase (TgSOD), positive control.

(C) Immunoblots of wild-type parasites and two clones (iKO1 and iKO2) of *Tg*REMIND-deficient lines grown in the presence or absence of ATc for 48 h and probed with anti-HA antibodies. ENO2 protein, a loading control.

(D) Immunoblots, as in (C), but probed with anti-*Tg*REMIND antibodies.

(E) Confirmation of *Tg*REMIND conditional depletion by confocal imaging using anti-HA and anti-*Tg*REMIND antibodies. Scale bar, 5 μm.

(F) Immunoblot of untreated or treated wild type, iKO-*Tg*REMIND, and complemented Comp-iKO2 probed with anti-HA and secondary antibodies Alexa Fluor 647 nm goat anti-rat.

(G) Immunoblots probed with anti-FLAG antibodies and secondary antibody Alexa Fluor Plus 800 nm goat anti-rabbit. F+G, merge of (F) and (G).

(H) Immunoblot with the loading materials as in (A) but probed with anti-*Tg*REMIND and ENO2 (loading control) antibodies.

To gain further insights into the nature and location of cellular membrane proteins interacting with *Tg*REMIND, we pulled down its partners using purified recombinant GST-full-length (FL) *Tg*REMIND, its F-BAR domain or REMIND, and total parasite protein extracted with Triton X-100, followed by mass spectrometry analyses. As shown in Figure S6A, all three or two baits share 118 (52%) of the 224 proteins pulled down. However, GST-REMIND, GST-(FL) *Tg*REMIND, and GST-F-BAR alone pulled down only 19 (8%), 28 (12%), and 59 (26%) proteins, respectively. Interestingly, we identified numerous proteins that were categorized as follows in Table S1: (1) 55 factors involved in lipid/protein trafficking and biogenesis of vesicles and organelles, (2) 12 ROP proteins, (3) 12 GRA proteins, (4) 4 MIC proteins, and (5) 26 cytoskeleton and microtubule components. This functional classification of all proteins identified by mass spectrometry revealed that some of the interactors play a role in trafficking of vesicle membranes from the ER to the Golgi apparatus, recycling from the ELC to the post-Golgi, and organelle biogenesis, in addition to regulators of membrane lipids and transporter/exchangers of membrane lipids (Table S1). As several ROP and GRA proteins were identified, these data agree with the co-distribution observed between *Tg*REMIND with ROP and GRA proteins, while no co-distribution was noticed with MIC proteins. We conclude that *Tg*REMIND, with its membrane-lipid-interacting F-BAR domain, may be involved in the formation of rhoptries and dense granules.

*Tg*REMIND silencing abrogates secretion of ROP and GRA proteins

We conditionally knocked out the *Tg*REMIND gene using the strategy in Figure 2A. We selected two positive knockout clones, which showed a perfect deletion of the endogenous target gene (Figure 2B). Treatment with ATc resulted in the disappearance of the *Tg*REMIND protein in the two knockout clones (iKO1 and iKO2), as revealed by western blots (Figures 2C and 2D) and confocal microscopy (Figure 2E). We complemented this mutant with the full-length (FL) FLAG-tagged-*Tg*REMIND (Figures 2F and 2G, see Comp-iKO2), which was introduced into the non-essential uracil phosphoryl transferase (UPRT) locus.[30] We confirmed the complementation of iKO-*Tg*REMIND mutants as HA-*Tg*REMIND and *Tg*REMIND-FLAG proteins were simultaneously expressed (Figure 2G, merge F+G, see the yellow

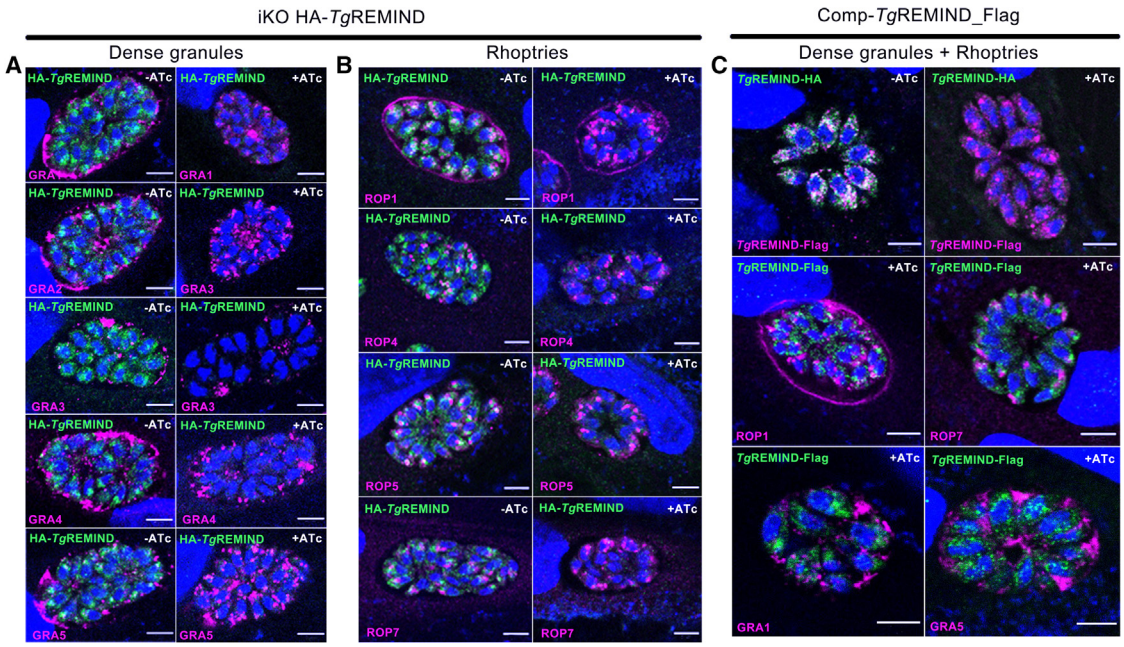

Figure 3. The conditional depletion of *Tg*REMIND abrogates the secretion of GRA proteins into the PVM and changes the distribution of ROP proteins

(A) In the presence of ATc, GRA1, GRA2, GRA3, GRA4, and GRA5 proteins lacked a strong fluorescence signal beneath the PVM of the *Tg*REMIND-depleted mutants (right). These GRA proteins were intensively present near the PVM of untreated mutants (left).

(B) Decrease in ROP1 protein in the PVM of *Tg*REMIND-depleted mutants with a total absence of signal in some PVM areas (top right), while in the untreated *Tg*REMIND mutants, the protein displays typical strong signal staining the PVM (top left and middle). Under the same conditions, the ROP4, ROP5, ROP7, and ROP1 proteins appear as punctate and fragmented signals (right) compared with the normal compacted signal of untreated mutants (left).

(C) Complementation of iKO-*Tg*REMIND-deficient mutants with ectopic full-length *Tg*REMIND-FLAG (Comp-*Tg*REMIND-FLAG) restored the normal decoration of ROP1 (middle left) and compacted apical signal of ROP7 (middle right). The complementation also rescued the intense staining of GRA1 and GRA5 beneath the PVM (bottom left and right). The top images correspond to the co-distribution of *Tg*REMIND-HA and Comp_*Tg*REMIND-FLAG proteins (top left), and *Tg*REMIND-HA was depleted from the conditional mutants as expected (top right). Scale bar, 5 μm.

band). Only *Tg*REMIND-FLAG protein was present under ATc treatment (Figure 2G, merge F+G, see the red band). In untreated iKO-*Tg*REMIND mutants, the five distinct GRA proteins GRA1, GRA2, GRA3, GRA4, and GRA5 were strongly accumulated peripherally and beneath the PVM and in the intravacuolar space of the intracellular mutants (Figure 3A, left images). These peripheral and intense signals of GRA proteins underneath the PVM disappeared from the ATc-treated mutants (Figure 3A, right images). Instead, the GRA signals accumulated in the residual bodies under ATc pressure (Figure 3A, right images). As expected, the ROP1 protein appeared to strongly and homogeneously decorate the PVM in the untreated mutants (Figure 3B, top left images). In contrast, in the ATc-treated mutants, the ROP1 fluorescence was weaker and sometimes discontinuous in all the treated vacuoles (Figure 3B, top right images). In addition, the fluorescence of ROP1, but also that of the ROP4, ROP5, and ROP7 proteins, known to be present in the PVM, was more punctate inside the ATc-treated mutants (Figure 3B, right) compared with untreated mutants (Figure 3B, left). These later observations may suggest an increase in ROP-containing vesicles. Indeed, *Tg*REMIND-depleted parasites often had smaller PVs, with a nearly 50% reduction in size and with a reduced number of intracellular parasites, indicating a replication defect (Figures 3A and 3B, right vs. left). Complementation of the iKO-*Tg*REMIND mutants with an FL *Tg*REMIND-FLAG protein restored the secretion of both GRA and ROP proteins, as indicated by their accumulation on the periphery of the PVM and in the membrane of the PV, respectively, and a normal vacuole size, even in the presence of ATc (Figure 3C).

Immunoelectron microscopy showed that immunogold staining of ROP1 was reduced inside the lumen of rhoptries in the ATc-treated mutants (Figure 4A, right, see enlargement inset) relative to untreated mutants (Figure 4A, left, magnification inset). We found that the number of immunocolloidal golds on the rare dense granules seen in the ATc-treated mutants was much lower than that of the untreated mutants, which contained many more dense granules with numerous immunocolloidal golds (Figure 4A, left vs. right, magnification insets). Biochemical analyses showed that depletion of *Tg*REMIND after ATc pressure led to an ~75% ± 2% ($p < 0.0001$) reduction in secretion of GRA1 protein from extracellular mutants that were incubated with propranolol,[31] known to trigger the release of GRA and MIC proteins in the extracellular medium (Figures 4B and 4C). In contrast, no decrease was observed in the MIC9 protein after ATc and propranolol treatment; instead, an ~30% ± 5% increase was observed (Figures 4B and 4D). However, the MIC9 protein in both pellets and supernatants of ATc-treated mutants appeared more intense than in the untreated parasites, suggesting that the

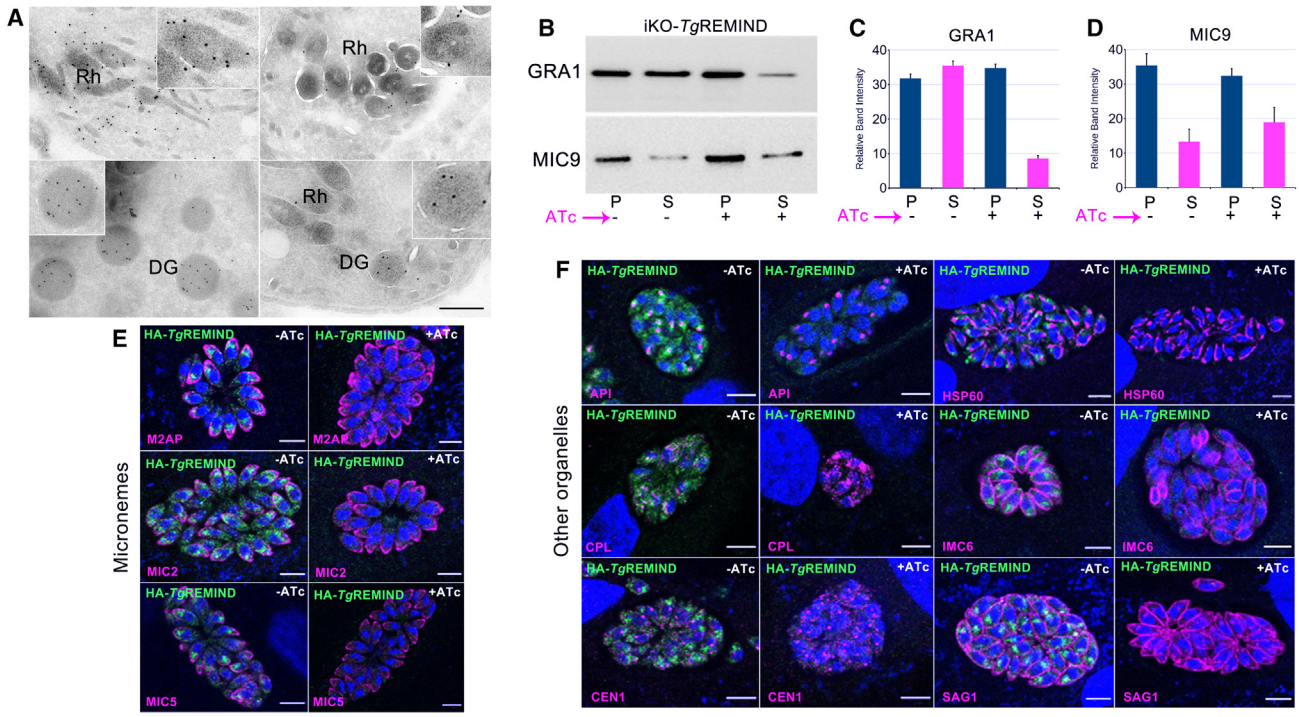

Figure 4. Phenotypic analysis of secretory and other organelles in *Tg*REMIND-depleted parasites

(A) Immunoelectron microscopy using untreated (left) or ATc-treated (right) iKO-*Tg*REMIND mutants followed by staining with anti-ROP1 (top) or anti-GRA1 (bottom) antibodies and revealed by immunogold secondary antibodies. Insets in the top right corners correspond to a magnification of one rhoptry or dense granule. Scale bar, 500 nm.

(B) One representative immunoblot showing GRA1 (top) and MIC9 (bottom) secretion of untreated vs. ATc-treated *Tg*REMIND-deficient parasites using induction of secretion with propranolol. P, pellet; S, supernatant.

(C and D) Quantification of GRA1 and MIC9 secretion from untreated and ATc-treated *Tg*REMIND mutants using induction of secretion with propranolol. Bars, n = 3 ± SD. *p < 0.05, **p < 0.01, and ***p < 0.001. P, pellet; S, supernatant.

(E) Confocal images of *Tg*REMIND-depleted parasites show the classical and normal pattern of micronemes for anti-MIC (M2AP, MIC2, and MIC5) antibodies before (left) and after (right) ATc treatment. Scale bar, 5μm.

(F) Subcellular localizations of the apicoplast (Atrx2, API), mitochondrion (HSP60), cathepsin L-containing compartment (CPL), inner complex membrane (IMC), centriole (CEN1), and plasma membrane (SAG1) markers were unchanged in the *Tg*REMIND-deficient mutant. Scale bar, 5 μm.

equivalent number of parasites loaded may be higher in ATc- vs. ATc-untreated materials. Therefore, this increase in MIC9 protein in the secretion of ATc-treated mutants was under low confidence ($p < 0.05$), suggesting that it may not be statistically significant. Furthermore, we confirmed that the apical fluorescence pattern of three other MICs, M2AP, MIC2, and MIC5, was unchanged in ATc-depleted vs. untreated iKO-*Tg*REMIND mutants (Figure 4E, right and left). Confocal imaging showed that all other intracellular organelles, such as the apicoplast (API), the mitochondrion (HSP60), the CPL-containing organelle (known to be involved in the maturation of MIC proteins), the inner membrane complex (IMC), the centriole (CEN), and plasma membrane (surface antigen 1 [SAG1]) were not affected by the depletion of *Tg*REMIND protein in these mutants (Figure 4F).

*Tg*REMIND is essential for organelle biogenesis in *T. gondii*

Multiple vacuoles containing between 16 and 32 parasites were analyzed by transmission electron microscopy. The untreated iKO-*Tg*REMIND parasites showed a lumen with electron-dense material in both their neck and the bulb subcompartment of rhoptries (Figures 5A and 5B). In contrast, the electron-dense club-shaped rhoptries in the *Tg*REMIND-depleted parasites appeared with a uniformly translucent lumen (Figure 5C, marked Rh). We confirmed that most *Tg*REMIND-depleted mutants lacked dense granules (Figures 5C and 5D), whereas the parental parasites containing functional *Tg*REMIND showed typical dense granules (Figure 5B, white stars). These data support the decrease in GRA proteins secreted in the periphery of the PVM of intracellular iKO-*Tg*REMIND mutants. These ultrastructural data also confirmed the equal presence of the flattened microneme organelles (marked Mn) at the apical end of both iKO-*Tg*REMIND-deficient mutants and *Tg*REMIND-expressing parasites (Figures 5A, 5B, and 5C), confirming no apparent defect in the morphology of micronemes in the absence of *Tg*REMIND. We also observed the presence of numerous round and flattened unknown vesicles in the lumen of the PV of *Tg*REMIND-depleted parasites but not in untreated mutants (Figure 5D, black arrows). However, there were no morphological differences seen for the conoid, Golgi apparatus

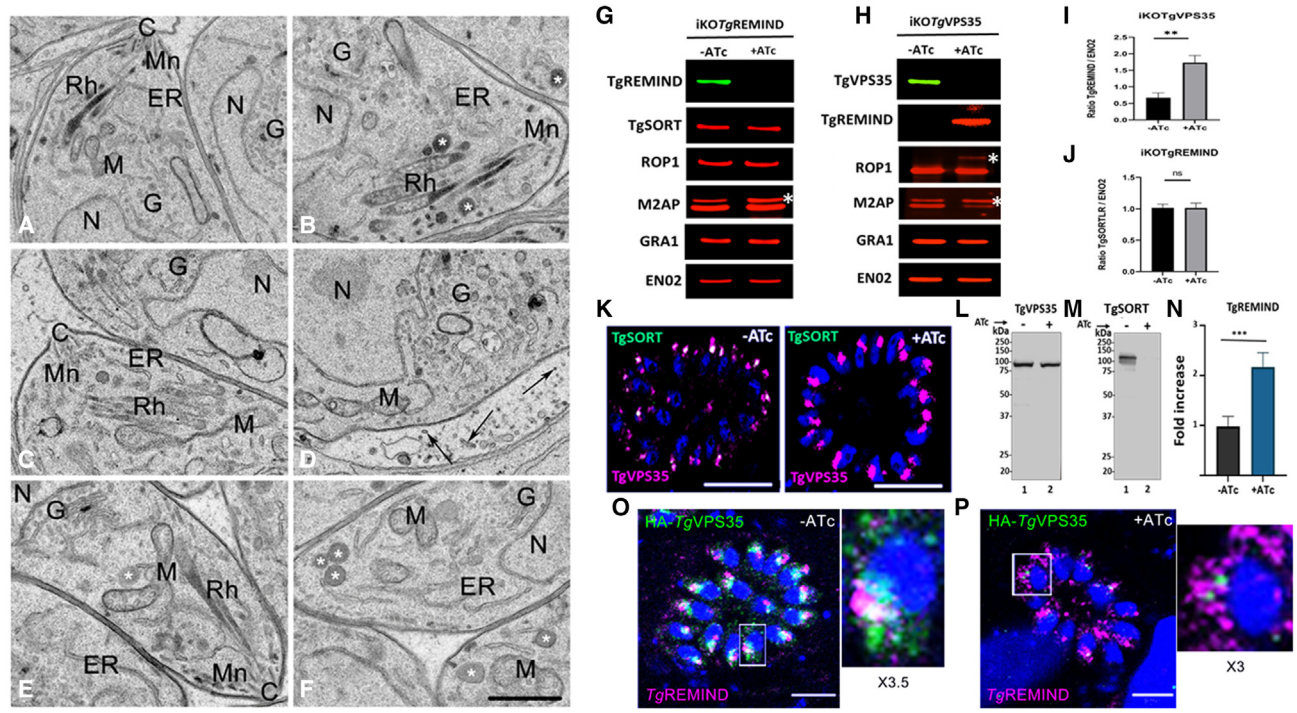

Figure 5. *Tg*REMIND is crucial for the biogenesis and functions of dense granules and rhoptries

(A and B) Transmission electron micrographs showing typical rhoptries (Rh), dense granules (white stars), and micronemes (Mn) in the untreated iKO-*Tg*REMIND mutants.

(C and D) Transmission electron micrographs of *Tg*REMIND-deficient mutants lacking dense granules and showing translucent rhoptries after 48 h of ATc treatment.

(E and F) Complementation of *Tg*REMIND-deficient mutants restored the presence of dense granules (white stars) and normal morphology of rhoptries (Rh). C, conoid; ER, endoplasmic reticulum; G, Golgi apparatus; M, mitochondrion; and N, nucleus. Scale bar, 500 nm.

(G) Immunoblots showing *Tg*SORT, ROP, GRA, and MIC protein levels in the ATc-treated and untreated iKO-*Tg*REMIND parasites. ENO2 was used as a loading control.

(H) Conditional disruption of *Tg*Vps35 gene led to an increase in *Tg*REMIND protein level. Inhibition of ROP and MIC processing and maturation was confirmed in *Tg*Vps35-deficient parasites. White star corresponds to unprocessed pro-proteins.

(I) Quantification showing a three-fold increase in *Tg*REMIND level in *Tg*Vps35-deficient parasites. Bars, n = 3 ± SD.

(J) Quantification showing that the *Tg*SORT level was unchanged in iKO-*Tg*REMIND mutants regardless of ATc treatment. Bars, n = 3 ± SD.

(K) Confocal images showing the expression of HA-*Tg*Vps35 after gene knockin into *Tg*SORT-deficient mutants after double homologous recombination in the UPRT locus. Immunofluorescence assay (IFA) was performed using anti-HA and anti-*Tg*SORT antibodies. Scale bars, 5 μm.

(L) Immunoblot demonstrating that the expression of HA-*Tg*Vsp35 protein was unchanged after ATc treatment or no treatment, as expected.

(M) Immunoblot confirming that the background of iKO-*Tg*SORT subjected to ATc treatment led to the disappearance of *Tg*SORT protein.

(N) Quantification of *Tg*REMIND protein level in the knockin of HA-*Tg*Vps35/iKO-*Tg*SORT after co-immunoprecipitation and semiquantitative mass spectrometry.

(O) Localization of the *Tg*REMIND protein in untreated *Tg*Vsp35-deficient mutants using anti-HA and anti-*Tg*REMIND antibodies. Zoom shows that *Tg*REMIND is in the vicinity of *Tg*Vps35. Scale bar, 5 μm.

(P) Localization of *Tg*REMIND in ATc-treated *Tg*Vps35-deficient mutants. Scale bar, 5 μm.

(marked G), ER, IMC, plasma membrane, and mitochondrion, as confirmed by the confocal imaging using specific antibodies for these classical organelles or compartments (Figure 4E). Furthermore, complementation of the iKO-*Tg*REMIND mutants rescued the presence of normal electron-dense rhoptries and dense granules that were again detected in these mutants even under the pressure of ATc (Figures 5E and 5F).

Crosstalk between *Tg*REMIND and the trafficking regulator *Tg*SORT-*Tg*Vps35 retromer complex in *T. gondii*

To investigate the role of *Tg*REMIND in ROP and MIC maturation when routed into the ELC, we performed comparative immunoblots using total protein extracts from our conditional iKO-*Tg*REMIND, iKO-*Tg*SORT, and iKO-*Tg*Vps35 mutants. We found no difference in pro-protein processing and maturation of ROP and MIC proteins in *Tg*REMIND-depleted parasites by ATc treatment compared with untreated *Tg*REMIND parasites (Figure 5G, white star). In contrast, we confirmed that ROP and MIC proteins were not processed to maturation in iKO-*Tg*Vps35 and iKO-*Tg*SORT mutants (Figures 5H and S5B, see white stars). Still, the level of *Tg*REMIND protein increased more than three-fold in ATc-treated iKO-*Tg*Vps35 parasites compared with untreated mutants (Figures 5H and 5I). No change was seen in *Tg*SORT protein level in iKO-*Tg*REMIND parasites (Figures 5G and 5J). The increased level of *Tg*REMIND protein was also observed in

ATc-treated iKO-*Tg*SORT parasites (Figure S6B). To confirm that *Tg*REMIND protein accumulated to at least a three-fold level under ATc treatment vs. untreated parasites, we performed coIP using cMyc-*Tg*Vps35 as bait (Figure 5N). We checked by immunoblotting that the transgenic *Tg*Vps35-cMyc parasites used for this coIP were devoid of *Tg*SORT protein under ATc pressure (Figures 5K and 5M). At the same time, the level of *Tg*Vps35-cMyc expression was unchanged, as expected (Figures 5K and 5L). Moreover, in the absence of either *Tg*Vps35 protein (Figure 5P) or *Tg*SORT (Figure S5C, right), *Tg*REMIND was more dispersed in the cytoplasm of the parasite with the loss of the concentrated signal of the protein on the top of the nucleus, where it partially co-localizes with rhoptries and dense granules. The signal of *Tg*Vps35-cMyc was partially co-distributed with *Tg*REMIND, indicating that an amount of *Tg*REMIND protein may be close to *Tg*Vps35-cMyc (Figure 5O). As expected, *Tg*SORT was also partially co-distributed with *Tg*REMIND (Figure S6C, left).

Spinning disk confocal microscopy coupled to live SR module revealed that fluorescence signals of *Tg*SORT partially intersected those of *Tg*REMIND, suggesting a crosstalk between the *Tg*SORT-*Tg*Vps35 retromer complex and *Tg*REMIND at the ELC (Video S1). Interestingly, this spinning disk confocal imaging with a better resolution revealed cytoplasmic vesicles that moved from the ER to the *trans*-Golgi network (TGN)/ELC before trafficking to the apical end where rhoptries and micronemes are located (Video S1). As *Tg*SORT is not essential for dense granule maturation,[20] we concluded that functional cooperation between *Tg*REMIND and the *Tg*Vps35 retromer complex may regulate the formation of vesicles whose contents are essential for the biogenesis of dense granules.

*Tg*REMIND binds to inositol phospholipids and is required for secretory organelle functions

To better understand the molecular mechanisms underlying *Tg*REMIND functions in *T. gondii*, we analyzed the model of the 3D structure of the full-length *Tg*REMIND protein made by AlphaFold2 (AF-S7W745). The F-BAR domain was modeled with very high confidence (blue in Figure 6A) and contained three long kinked α helices. This domain, further modeled as a homodimer (F-BAR(A) and F-BAR(B)) using AlphaFold2-multimer, forms a well-packed, crescent-shaped, symmetrical, six-helix bundle (Figure 6A). In addition, the REMIND was also predicted with very high (blue) to high (cyan color) confidence and appears at the two extremities of the antiparallel homodimer (Figure 6A). It corresponds to an original 3D structure, which folds as a superhelix of consecutive helices (secondary structures are shown in rainbow color from the N to the C terminus; Figure 6B; see the Figure S7 legend for details). Notably, the REMIND comprises two lobes, the C-terminal lobe starting at strand S7 showing the highest sequence conservation across the REMIND family (Figure S4). This C-terminal lobe also contains a variable region, generally predicted by AlphaFold2 with high or very high confidence, which interacts with other domains of the proteins (indicated by gray ribbons in Figure S7). In *Tg*REMIND, this region directly contacts the extremities of the F-BAR domains (Figures 6A and 6B). In human MADD, this region (death domain[32]) interacts with the downstream Pleckstrin homology (PH)-like domain (Figure S7), known to bind to phosphatidylinositol lipids PI3,4,5P2 and PI4,5P2.[33] These findings suggest that the REMIND may have a regulatory function on the F-BAR domain. To further demonstrate how the REMIND may influence the activity of the F-BAR domain, we complemented the *T. gondii* iKO-*Tg*REMIND mutants by transiently expressing plasmids encoding only the F-BAR domain or only the REMIND and compared this with the full-length *Tg*REMIND protein expression under the same experimental conditions (Figure 6C). When these complemented parasites were incubated with ATc to deplete the endogenous *Tg*REMIND protein, neither the F-BAR domain alone nor the REMIND was able to rescue the secretion of ROP1 (Figure 6C, middle and left) and GRA1 (Figure 6D, middle and left) into both the periphery and the membrane of the PV of intracellular iKO-*Tg*REMIND-depleted mutants. In contrast, complementation with the FL-*Tg*REMIND perfectly restored ROP1 and GRA1 secretion into both the periphery and the membrane of the PV (Figures 6C and 6D, right). These data demonstrate that the F-BAR domain and REMIND are crucial for *Tg*REMIND functions. We then fused the F-BAR, REMIND, and entire *Tg*REMIND to GST at their N termini (Figure 6E), which were expressed in *E. coli* and purified (Figures 6F and 6G). The FL *Tg*REMIND strongly binds to PIP2 species, with more intense binding to PI4,5P2, as shown by lipid overlay experiments (Figure 6H). These data are consistent with the biochemical behaviors of mammalian F-BAR-containing domain proteins that are known to bind multiple phosphoinositides such as PI3P, PI(3,5)P2, and PI(3,4,5)P2 with variable affinities.[34] Under our experimental conditions, the *T. gondii* F-BAR domain exhibited weaker binding to PIP2 species (Figure 6H). Still, this binding level increased in intensity when higher amounts of recombinant F-BAR domain alone were used. We observed a similar binding to PIP2 lipids when these recombinant proteins were fused to a smaller HA or cMyc-Tag. No binding to PIP2 lipids was observed for the recombinant REMIND alone (Figure 6H).

The absence of *Tg*REMIND impairs host cell infection

Although transient expression was obtained for all three FLAG epitope-tagged F-BAR, REMIND, and FL-*Tg*REMIND constructs, we could not obtain stable parasite lines containing the plasmid F-BAR domain alone. This confirms that the REMIND is required in association with the F-BAR domain to obtain viable and stable complemented parasite lines. Interestingly, transgenic stable parasite lines can be generated using the REMIND alone, suggesting that the F-BAR domain alone is toxic to *T. gondii*. Next, we examined the functional role of *Tg*REMIND in host infection by *T. gondii*. In the presence of ATc, iKO-*Tg*REMIND mutants were severely impaired in host cell invasion (Figure 7A), and complementation with FL-*Tg*REMIND restored their invasion capability to that of the untreated mutants (Figure 7A). In contrast, complementation with the REMIND alone failed to complement the iKO mutants (Figure 7A) efficiently. These latest data confirmed that F-BAR and REMIND are necessary for *Tg*REMIND functions in *T. gondii*. We observed a slight increase in host cell invasion by the mutants complemented with REMIND alone compared with the *Tg*REMIND-depleted mutants (Figure 7A). Finally, to assess the essentiality of *Tg*REMIND in host infection, we tested the ability of parasites to

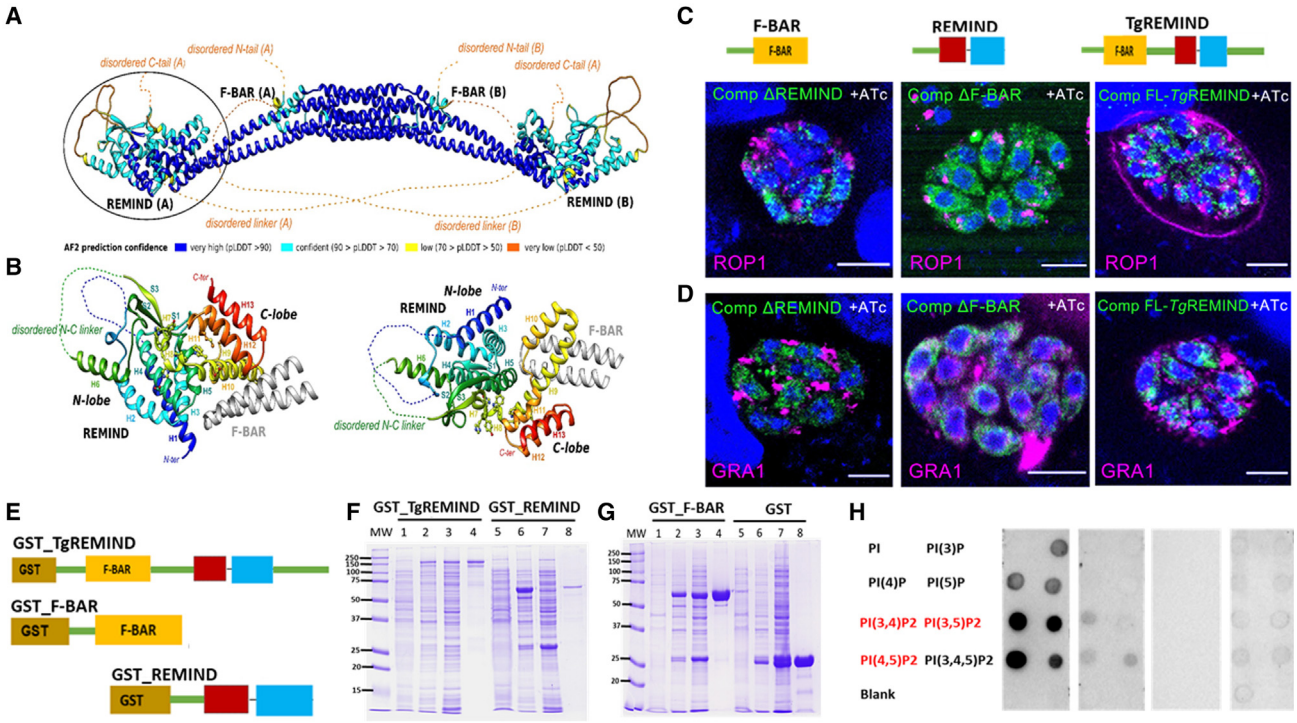

Figure 6. The F-BAR-containing *Tg*REMIND protein requires its C-terminal REMIND for efficient binding to PI2P lipids

(A) A 3D structure model of the *Tg*REMIND dimer, with residues colored according to the AlphaFold2 pLDDT. The disordered segments are represented with orange dashed lines. The 3D structure models of the whole protein monomers (AF-S7W745) are superimposed on the 3D structure model of the *Tg*REMIND F-BAR dimer (aa 80–345). The conformation of the helical hairpin of the F-BAR domain (aa 214–259) interacting with the REMIND is similar between the F-BAR dimer and the whole protein monomers (0.24 Å on 46 Cα atoms).

(B) Focus on the REMIND (left, encircled domain) and on the right, with a 90° rotation, colored from blue (N terminus) to red (C terminus).

(C) Schematic representation of FL_*Tg*REMIND-FLAG, F-BAR-FLAG, and REMIND-FLAG plasmids for transient transfection and confocal images showing that the N-terminal F-BAR domain alone or the C-terminal REMIND cannot restore the presence of ROP1 in the PVM in *Tg*REMIND-deficient mutants (left and middle). Only complementation with the full-length *Tg*REMIND protein restored secretion ROP1 in the PVM (right). Scale bars, 3 μm.

(D) Confocal images show that the N-terminal F-BAR domain alone or the C-terminal REMIND cannot restore a strong GRA1 signal beneath the PVM of *Tg*REMIND-deficient mutants (left and middle). Only complementation with the full-length *Tg*REMIND protein restored GRA1 secretion beneath the PVM in *Tg*REMIND-deficient parasites under ATc pressure (right). Scale bars, 3 μm.

(E) Schematic representation of plasmids used to express recombinant GST_*Tg*REMIND, GST_F-BAR, and GST_REMIND proteins in *Escherichia coli*.

(F and G) SDS-PAGE and Coomassie blue staining of expression and purification of recombinant GST_*Tg*REMIND, GST_F-BAR, and GST_REMIND. Lanes 1 and 5, uninduced transformed bacteria; 2 and 6, IPTG-induced recombinant bacteria; 3 and 7, total protein extract after sonication; 4 and 8, GST-affinity purification.

(H) Lipid overlay experiments using the purified recombinant proteins and different PIP2 lipid species.

form plaques on host cell monolayers, which correspond to multiple rounds of parasite entry and egress, ensuring parasite dissemination and host cell lysis. These assays also measure the overall growth rate of the parasites based on the plaque sizes. Interestingly, the plaque size was reduced to less than 10% when the iKO-*Tg*REMIND mutants complemented with REMIND alone were treated with ATc relative to untreated mutants (Figure 7B, bottom), thus suggesting a slower growth rate and parasite entry within new host cells in the absence of fully functional *Tg*REMIND. The wild-type parasites grew normally and developed large and equal-sized plaques in the absence and presence of ATc (Figure 7B). In the presence of ATc, plaque formation was utterly blocked in *Tg*REMIND-deficient parasites, whereas the growth of iKO-*Tg*REMIND lines gave rise to normal plaque sizes only in the absence of ATc (Figure 7B). iKO mutants complemented with FL-*Tg*REMIND protein formed plaques with normal number and large size regardless of the presence of ATc (Figure 7B), confirming that the absence of F-BAR is detrimental to the functions of *Tg*REMIND in *T. gondii*.

DISCUSSION

In this study, we describe that the *Tg*REMIND protein, which contains both an F-BAR domain and REMIND, is indispensable for the proper function of rhoptries and dense granules. *Tg*REMIND belongs to the F-BAR family and has the dimer crescent or banana-shape form that is characteristic of this family.[25,26,35] The F-BAR domain in *Tg*REMIND is similar to the FES-CIP4 homology (FCH) domain, which is the archetypal feature of all known F-BAR proteins.[36] F-BAR-containing proteins are a family of α-helical membrane-binding modules that can detect, induce, and regulate membrane curvature and thereby play essential roles in biological processes, such as endocytosis, exocytosis, regulation of the actin cytoskeleton, cell motility,

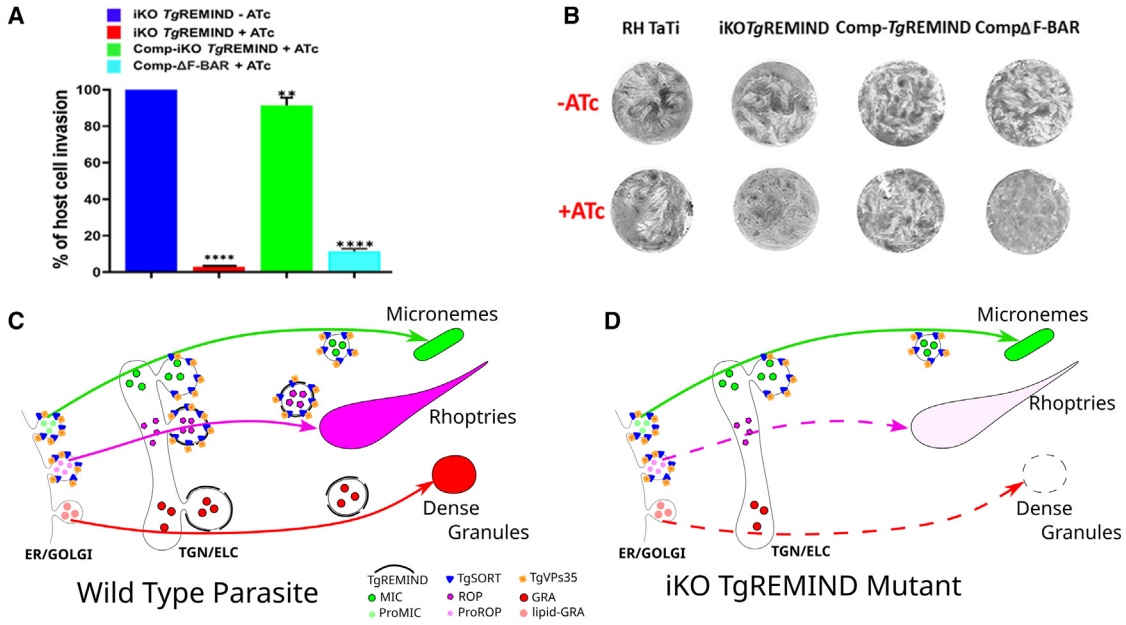

Figure 7. *Tg*REMIND is essential for host cell infection

(A) Host cell invasion is impaired in iKO-*Tg*REMIND mutants after ATc treatment. Complementation with the full-length *Tg*REMIND protein restored host cell invasion. In contrast, complementation with the C-terminal domain alone gives rise to a lower rate of cell host invasion compared with parental parasites and complemented mutants with full-length *Tg*REMIND. Bars, n = 3 ± SD. *p < 0.01 and **p < 0.0001.

(B) Inhibition of plaque formation of *Tg*REMIND-depleted mutants (iKO-*Tg*REMIND). Parental (RH TaTi) and complemented (Comp-*Tg*REMIND) parasites show plaque formation, whereas complemented REMIND alone (CompΔF-BAR), parasites show only tiny plaques.

(C and D) Models of how *Tg*REMIND functions in the biogenesis and secretion of *T. gondii* dense granules and rhoptries.

and signaling.[25,37] Although the functions of some individual F-BAR proteins have been studied using recombinant proteins and *in vitro* model systems,[38,39] many questions remain unanswered, such as how the accompanying domains located at the C terminus regulate the precise function of the F-BAR domain and how these proteins are regulated in living cells.

We used predictive structural and biochemical analyses, gene disruption, and complementation studies to show that *Tg*REMIND is essential for host cell infection and parasite dissemination. Indeed, we found that rhoptries are morphologically and functionally altered and the number of dense granules decreased in *Tg*REMIND-deficient parasites. Consequently, the secretions of ROP and GRA proteins were severely impaired. We observed a significant drop in the localization of ROP proteins beneath the PVM and inside the PV of *Tg*REMIND-depleted mutants. A complete absence of ROP1 protein in some portions of the PVM was evidenced in addition to a more fragmented signal for ROP4, ROP5, and ROP7, including ROP1 protein. The presence of ROP proteins outside and in the close vicinity of rhoptries was seen by immunoelectron microscopy in these mutants. In contrast, these proteins can be correctly detected in the lumen of rhoptries in the parental parasites. In the absence of *Tg*REMIND, dense granules are not formed or rarely seen, with fewer GRA proteins inside these organelles. These data suggest *Tg*REMIND as a critical factor in the formation and functions of these two vital secretory organelles, and this requires the concomitant functions of both F-BAR and REMIND as demonstrated by complementation of the conditional *Tg*REMIND mutants. As rhoptries and dense granules are known to be involved in the formation of the PV, a niche in which the parasites grow and multiply by obtaining nutrients from infected cells, we suggest that *Tg*REMIND is a regulator of formation of membrane vesicles containing components destined for rhoptries and dense granules. In contrast, the absence of *Tg*REMIND had no impact on the morphology and secretion of micronemes. Altogether, these observations indicate that the biogenesis of micronemes involved other regulators and pathways independent from those of *Tg*REMIND. This conclusion is supported by the recent notion that micronemes are not only formed *de novo* by the newly born daughter parasites but also efficiently recycled from the mother parasites.[20] Therefore, it is unlikely that *Tg*REMIND may have an impact on the morphology and secretion of mature and recycled micronemes in the parasites. However, we cannot entirely rule out that *Tg*REMIND may indirectly influence the functions of micronemes, as we showed that the protein binds to phosphorylated inositides. It has been described that phosphorylated inositides can regulate Ca^{2+} homeostasis through the ER and Golgi network apparatus, thus enabling the parasite to generate its own IP3-dependent Ca^{2+} signaling, which is known to govern the motility, egress, and invasion processes.[40] Interestingly, we identified, by mass spectrometry, several ER and Golgi proteins pulled down by *Tg*REMIND. In addition, our preliminary observations suggested that parasite motility may be affected in the *Tg*REMIND-depleted mutants. However, as these mutants replicated more slowly than the parental strain and egressed from the infected host cells later compared with the parental parasites, it is

difficult to distinguish between a potential defect in parasite gliding motility vs. parasites that are dead or dying and thereby are unable to exhibit active motility.

The presence of the REMIND domain at the C terminus, in association with the F-BAR domain at the N terminus, is indispensable for *Tg*REMIND protein to function properly *in vivo*. We also showed that *Tg*REMIND is a membrane-associated component, and the entire *Tg*REMIND protein efficiently interacts *in vitro* with different phosphorylated inositides or PIP2 lipids (PI3,4,5P2, PI3,4P2, P3,5P2, and PI4,5P2) under our experimental conditions. These last findings are consistent with the biochemical properties of other mammalian F-BAR-containing proteins that also bind to different phosphoinositides with an affinity of PI3,4,5P2 > PI3,4P2 > PI3P using giant unilamellar vesicles (GUVs) and confocal microscopy.[34] Therefore, we conclude that the lack of specificity toward some PI species is consistent with the promiscuity observed for the BAR family domains, which recognize broad physical properties of the membrane mediated through electrostatic interactions.[34] This binding generally needs adjacent domains to enhance specificity and/or affinity.[35] It is worth noting that the REMIND, identified for the first time in this study, is predicted to fold as a superhelix, like ENTH domains, which bind $PI(4,5)P_2$ through the folding of a specific helix upon binding.[36] Further experimental characterization is needed to understand the molecular mechanism of *Tg*REMIND-PIP2 interactions, as the current 3D structure models cannot predict this. Worth noting is that the REMIND was also found in other eukaryotic proteins with distinct domain architectures, being in particular associated with DENN and TBC domains, which are known as regulators of Rab small GTPases involved in intracellular trafficking.[37] The REMIND is thus likely to play a specific role in this context, which remains to be further explored. It is tempting to speculate that, like other mammalian F-BAR-containing proteins, *Tg*REMIND may sculpt vesicles containing ROP and GRA proteins by inhibiting lateral diffusion, thus generating extremely stable protein-lipid microdomains, as already described for other F-BAR-containing proteins.[34] In the absence of *Tg*REMIND, these vesicles may be destabilized, leading to the abnormal presence of ROP and GRA proteins in the cytoplasm of the mutants. In other words, we hypothesize that the F-BAR domain scaffolds may generate stable *Tg*REMIND-PIP2-harboring vesicles that are likely to play important roles in the biogenesis of rhoptries and dense granules in *T. gondii*. The presence of actin, myosin, and microtubule proteins suggests that vesicles formed by *Tg*REMIND may traffic along actin filaments or microtubules to reach their destination, similar to F-BAR-containing proteins in mammalian cells.[36,41–44] Notably, the transport and secretion of dense granules depend on actin filaments and myosin F,[18] which were also present in our proteomics data. The requirement of REMIND combined with F-BAR to fully complement the *Tg*REMIND-deficient mutants and our inability to obtain viable parasite stable lines expressing the F-BAR alone suggest that *Tg*REMIND functions must be tightly regulated in *T. gondii*. We propose a model in which *Tg*REMIND protein containing F-BAR and REMIND forms vesicles that drive anterograde transport containing components such as lipids and proteins destined for rhoptries and dense granules during their biogenesis (Figure 7C). Our data show that deficits in *Tg*REMIND function led to morphological perturbations of rhoptries and decreased number of dense granules, accompanied by a loss in dense granules and rhoptry exocytosis (Figure 7D). Taken together, our data support a role for *Tg*REMIND in the biogenesis of rhoptries and dense granules. Despite advances in electron microscopy, the biogenesis of dense granules is less well understood in *T. gondii*. It probably involves several proteins, including *Tg*Vps11, *Tg*Vps9, and *Tg*Vps35.[24,45,46] Our findings demonstrate that *Tg*REMIND, which can bind PIP2 lipids, likely plays a role in dense granule biogenesis, which is more complex than a simple budding of fully matured dense granules from the TGN, as generally reported.[18] It is generally admitted that, like GRA proteins, the SAG proteins would also bud from the TGN and transport directly to the plasma membrane. Nevertheless, we found that the SAG1 proteins are correctly trafficked to the plasma membrane, thus suggesting that SAG and GRA proteins may follow, at some level, a different trafficking pathway. Our ability to conditionally extinguish *Tg*REMIND expression and complement these mutants will allow functional dissection of regulators of *Tg*REMIND protein. This will help shed more light on the essential sorting mechanism involved in the biogenesis of secretory organelles in *T. gondii*.

Limitations of this study

First, even though 3D structure models of the F-BAR domain are accurate, the shape of the dimeric helical bundle linked to the functional properties of the assembly could only be approximated in the modeling. Second, the REMIND belongs to a novel family and is modeled with globally lower confidence and some uncertainties. Third, the F-BAR domain and the REMIND are separated by a long linker, which is predicted as disordered, and its role in regulating the two other domains has not been determined in this work. Fourth, our attempts to crystallize *Tg*REMIND, F-BAR, and REMIND failed because when the GST tag is removed, the recombinant proteins are unstable and precipitated, probably because of their hydrophobic properties required for binding to lipids. Finally, future works are needed to define the exact molecular basis of *Tg*REMIND-PIP2 lipid interactions. This will require developing new tools, such as sensors determining the subcellular distribution of PIP2 species in the different compartments of the parasites and new methods deciphering the dynamics of lipids and vesicles in living parasites.

STAR★METHODS

Detailed methods are provided in the online version of this paper and include the following:

- KEY RESOURCES TABLE
- RESOURCE AVAILABILITY
  - Lead contact
  - Materials availability
  - Data and code availability
- EXPERIMENTAL MODEL AND STUDY PARTICIPANT DETAILS
  - Growth of host cells and parasite strains

SUPPLEMENTAL INFORMATION

Supplemental information can be found online at https://doi.org/10.1016/j.celrep.2023.113601.

ACKNOWLEDGMENTS

We thank our colleagues who generously provided invaluable antibodies for this study. In addition, we are grateful to Omar Ndao and Scott Thomas for technical assistance; members of the Gif Imaging Facility (I2BC, CNRS), Cynthia Dupas for electron microscopy, Romain Le Bars and Sandrine Lecart for the training and help on confocal microscopy; and other members of the lab, Ariane Honfozo and Mahendra Jamdhade, for their fruitful discussions; and Jeroen P.J. Saeij (University of Davis, California) for help with editing of the manuscript. This work was supported by a PhD fellowship from the Campus France, I2BC (CNRS) and WAEMU to R.H. and by financial support from the Agence Nationale de la Recherche grant ANR-19-CE44-0006 to S.T.

AUTHOR CONTRIBUTIONS

R.H., L.O.S., T.D.A., A.D., and C.B. performed the experiments. Y.H., C.M.A., L.A.F., C.S., T.B.-F., and I.C. contributed reagents/materials/analysis tools. L.O.S., T.D.A., C.B., C.S., and S.T. performed data analysis. S.T. conceived and designed the experiments. R.H., L.O.S., Y.H., I.C., and S.T. wrote the first draft. L.O.S., I.C., C.S., Y.H., and S.T. wrote the revised version. S.T. supervised the work, acquired funding, and wrote the original draft. All authors approved the content and submission of the paper.

DECLARATION OF INTERESTS

The authors declare that they have no competing financial interests.

Received: March 20, 2023
Revised: October 25, 2023
Accepted: December 4, 2023

REFERENCES

1. McAuley, J.B. (2014). Congenital Toxoplasmosis. J. Pediatric Infect. Dis. Soc. *3*, S30–S35.
2. Milne, G., Webster, J.P., and Walker, M. (2020). An underestimated threat? Trends Parasitol. *36*, 959–969.
3. Montoya, J.G., and Liesenfeld, O. (2004). Lancet *363*, 1965–1976.
4. Halonen, S.K., and Weiss, L.M. (2013). Handb. Clin. Neurol. *114*, 125–145.
5. Wang, Y., Sangaré, L.O., Paredes-Santos, T.C., and Saeij, J.P.J. (2020). *Toxoplasma* mechanisms for delivery of proteins and uptake of nutrients across the host-pathogen interface. Annu. Rev. Microbiol. *74*, 567–586.
6. Gubbels, M.-J., and Duraisingh, M.T. (2012). Evolution of apicomplexan secretory organelles. Int. J. Parasitol. *42*, 1071–1081.
7. Tagoe, D.N.A., Drozda, A.A., Falco, J.A., Bechtel, T.J., Weerapana, E., and Gubbels, M.-J. (2021). Ferlins and TgDOC2 in *Toxoplasma* microneme, rhoptry and dense granule secretion. Life *11*, 217.
8. Meissner, M., Reiss, M., Viebig, N., Carruthers, V.B., Toursel, C., Tomavo, S., Ajioka, J.W., and Soldati, D. (2002). A family of transmembrane microneme proteins of *Toxoplasma gondii* contain EGF-like domains and function as escorters. J. Cell Sci. *115*, 563–574.
9. Taylor, S., Barragan, A., Su, C., Fux, B., Fentress, S.J., Tang, K., Beatty, W.L., Hajj, H.E., Jerome, M., Behnke, M.S., et al. (2006). A secreted serine-threonine kinase determines virulence in the eukaryotic pathogen *Toxoplasma gondii*. Science *314*, 1776–1780.
10. Saeij, J.P.J., Coller, S., Boyle, J.P., Jerome, M.E., White, M.W., and Boothroyd, J.C. (2007). *Toxoplasma* co-opts host gene expression by injection of a polymorphic kinase homologue. Nature *445*, 324–327.
11. Boothroyd, J.C., and Dubremetz, J.-F. (2008). Kiss and spit: the dual roles of *Toxoplasma* rhoptries. Nat. Rev. Microbiol. *6*, 79–88.
12. Behnke, M.S., Fentress, S.J., Mashayekhi, M., Li, L.X., Taylor, G.A., and Sibley, L.D. (2012). The polymorphic pseudokinase ROP5 controls virulence in *Toxoplasma gondii* by regulating the active kinase ROP18. PLoS Pathog. *8*, e1002992.
13. Kremer, K., Kamin, D., Rittweger, E., Wilkes, J., Flammer, H., Mahler, S., Heng, J., Tonkin, C.J., Langsley, G., Hell, S.W., et al. (2013). An overexpression screen of *Toxoplasma gondii* Rab-GTPases reveals distinct transport routes to the micronemes. PLoS Pathog. *9*, e1003213.
14. Gold, D.A., Kaplan, A.D., Lis, A., Bett, G.C.L., Rosowski, E.E., Cirelli, K.M., Bougdour, A., Sidik, S.M., Beck, J.R., Lourido, S., et al. (2015). The *Toxoplasma* dense granule proteins gra17 and gra23 mediate the movement of small molecules between the host and the parasitophorous vacuole. Cell Host Microbe *17*, 642–652.
15. Huynh, M.-H., Rabenau, K.E., Harper, J.M., Beatty, W.L., Sibley, L.D., and Carruthers, V.B. (2003). Rapid invasion of host cells by *Toxoplasma* requires secretion of the MIC2-M2AP adhesive protein complex. EMBO J. *22*, 2082–2090.
16. Harper, J.M., Huynh, M.H., Coppens, I., Parussini, F., Moreno, S., and Carruthers, V.B. (2006). A cleavable propeptide influences *Toxoplasma* infection by facilitating the trafficking and secretion of the TgMIC2-M2AP invasion complex. Mol. Biol. Cell *17*, 4551–4563.
17. Butcher, B.A., Fox, B.A., Rommereim, L.M., Kim, S.G., Maurer, K.J., Yarovinsky, F., Herbert, D.R., Bzik, D.J., and Denkers, E.Y. (2011). *Toxoplasma* gondii rhoptry kinase ROP16 activates STAT3 and STAT6 resulting in cytokine inhibition and arginase-1-dependent growth control. PLoS Pathog. *7*, e1002236.
18. Griffith, M.B., Pearce, C.S., and Heaslip, A.T. (2022). Dense granule biogenesis, secretion, and function in *Toxoplasma gondii*. J. Eukaryot. Microbiol. *69*, e12904.
19. Tomavo, S., Slomianny, C., Meissner, M., and Carruthers, V.B. (2013). Protein trafficking through the endosomal system prepares intracellular parasites for a home invasion. PLoS Pathog. *9*, e1003629.
20. Periz, J., Del Rosario, M., McStea, A., Gras, S., Loney, C., Wang, L., Martin-Fernandez, M.L., and Meissner, M. (2019). A highly dynamic F-actin network regulates transport and recycling of micronemes in *Toxoplasma gondii* vacuoles. Nat. Commun. *10*, 4183.
21. Ngô, H.M., Yang, M., Paprotka, K., Pypaert, M., Hoppe, H., and Joiner, K.A. (2003). AP-1 in *Toxoplasma* mediates biogenesis of the rhoptry

secretory organelle form a post-Golgi compartment. J. Biol. Chem. *278*, 5343–5352.

22. Sloves, P.J., Delhaye, S., Mouveaux, T., Werkmeister, E., Slomianny, C., Hovasse, A., Dilezitoko Alayi, T., Callebaut, I., Gaji, R.Y., Schaeffer-Reiss, C., et al. (2012). *Toxoplasma* sortilin-like receptor regulates protein transport and is essential for apical secretory organelle biogenesis and host infection. Cell Host Microbe *11*, 515–527.
23. Honfozo, A., Ghouil, R., Alayi, T.D., Ouldali, M., Arteni, A.-A., Atindehou, C.M., Fanou, L.A., Hathout, Y., Zinn-Justin, S., and Tomavo, S. (2023). The luminal domain of *Toxoplasma gondii* sortilin adopts a ring-shaped structure exhibiting motifs specific to apicomplexan parasites. Front. Parasitol. *2*.
24. Sangaré, L.O., Alayi, T.D., Westermann, B., Hovasse, A., Sindikubwabo, F., Callebaut, I., Werkmeister, E., Lafont, F., Slomianny, C., Hakimi, M.A., et al. (2016). Unconventional endosome-like compartment and retromer complex in *Toxoplasma* gondii govern parasite integrity and host infection. Nat. Commun. *7*, 11191.
25. Shimada, A., Niwa, H., Tsujita, K., Suetsugu, S., Nitta, K., Hanawa-Suetsugu, K., Akasaka, R., Nishino, Y., Toyama, M., Chen, L., et al. (2007). Curved EFC/F-BAR domain dimers are joined end to end into a filament for membrane invagination in endocytosis. Cell *129*, 761–772.
26. Henne, W.M., Kent, H.M., Ford, M.G.J., Hegde, B.G., Daumke, O., Butler, P.J.G., Mittal, R., Langen, R., Evans, P.R., and McMahon, H.T. (2007). Structure and analysis of FCHo2 F-BAR domain: a dimerizing and membrane recruitment module that effects membrane curvature. Structure *15*, 839–852.
27. Huynh, M.-H., and Carruthers, V.B. (2009). Tagging of endogenous genes in a *Toxoplasma gondii* strain lacking Ku80. Eukaryot. Cell *8*, 530–539.
28. Kim, H., Botelho, S.C., Park, K., and Kim, H. (2015). Use of carbonate extraction in analyzing moderately hydrophobic transmembrane proteins in the mitochondrial inner membrane. Protein Sci. *24*, 2063–2069.
29. Breinich, M.S., Ferguson, D.J.P., Foth, B.J., van Dooren, G.G., Lebrun, M., Quon, D.V., Striepen, B., Bradley, P.J., Frischknecht, F., Carruthers, V.B., and Meissner, M. (2009). A dynamin is required for the biogenesis of secretory organelles in *Toxoplasma gondii*. Curr. Biol. *19*, 277–286.
30. Fox, B.A., and Bzik, D.J. (2002). De novo pyrimidine biosynthesis is required for virulence of *Toxoplasma gondii*. Nature *415*, 926–929.
31. Bullen, H.E., Jia, Y., Yamaryo-Botté, Y., Bisio, H., Zhang, O., Jemelin, N.K., Marq, J.B., Carruthers, V., Botté, C.Y., and Soldati-Favre, D. (2016). Phosphatidic acid-mediated signaling regulates microneme secretion in *Toxoplasma*. Cell Host Microbe *19*, 349–360.
32. Schievella, A.R., Chen, J.H., Graham, J.R., and Lin, L.L. (1997). MADD, a novel death domain protein that interacts with the type 1 tumor necrosis factor receptor and activates mitogen-activated protein kinase. J. Biol. Chem. *272*, 12069–12075.
33. Singh, N., Reyes-Ordoñez, A., Compagnone, M.A., Moreno, J.F., Leslie, B.J., Ha, T., and Chen, J. (2021). Redefining the specificity of phosphoinositide-binding by human PH domain-containing proteins. Nat. Commun. *12*, 4339.
34. Zhao, H., Michelot, A., Koskela, E.V., Tkach, V., Stamou, D., Drubin, D.G., and Lappalainen, P. (2013). Membrane-sculpting BAR domains generate stable lipid microdomains. Cell Rep. *4*, 1213–1223.
35. Heath, R.J.W., and Insall, R.H. (2008). F-BAR domains: multifunctional regulators of membrane curvature. J. Cell Sci. *121*, 1951–1954.
36. Aspenström, P. (2009). Roles of F-BAR/PCH proteins in the regulation of membrane dynamics and actin reorganization. Int. Rev. Cell Mol. Biol. *272*, 1–31.
37. Masuda, M., Takeda, S., Sone, M., Ohki, T., Mori, H., Kamioka, Y., and Mochizuki, N. (2006). Endophilin BAR domain drives membrane curvature by two newly identified structure-based mechanisms. EMBO J. *25*, 2889–2897.
38. Simunovic, M., Voth, G.A., Callan-Jones, A., and Bassereau, P. (2015). When physics takes over: BAR proteins and membrane curvature. Trends Cell Biol. *25*, 780–792.
39. Snider, C.E., Wan Mohamad Noor, W.N.I., Nguyen, N.T.H., Gould, K.L., Suetsugu, S., and Suetsugu, S. (2021). The state of F-BAR domains as membrane-bound oligomeric platforms. Trends Cell Biol. *31*, 644–655.
40. Ren, B., Liang, X., Brouwers, J.F., Miron, R.C., Shen, B., and Gupta, N. (2023). Synthesis vs. salvage of ester- and ether-linked phosphatidylethanolamine in the intracellular protozoan pathogen *Toxoplasma gondii*. Commun. Biol. *6*, 306.
41. Moravcevic, K., Oxley, C.L., and Lemmon, M.A. (2012). Conditional peripheral membrane proteins: facing up to limited specificity. Structure *20*, 15–27.
42. Ford, M.G.J., Mills, I.G., Peter, B.J., Vallis, Y., Praefcke, G.J.K., Evans, P.R., and McMahon, H.T. (2002). Curvature of clathrin-coated pits driven by epsin. Nature *419*, 361–366.
43. Müller, M.P., and Goody, R.S. (2017). Molecular control of Rab activity by GEFs, GAPs and GDI. Small GTPases *9*, 5–21.
44. Peter, B.J., Kent, H.M., Mills, I.G., Vallis, Y., Butler, P.J.G., Evans, P.R., and McMahon, H.T. (2004). BAR domains as sensors of membrane curvature: the amphiphysin BAR structure. Science *303*, 495–499.
45. Morlon-Guyot, J., Pastore, S., Berry, L., Lebrun, M., and Daher, W. (2015). *Toxoplasma gondii* Vps11, a subunit of HOPS and CORVET tethering complexes, is essential for the biogenesis of secretory organelles. Cell Microbiol. *17*, 1157–1178.
46. Sakura, T., Sindikubwabo, F., Oesterlin, L.K., Bousquet, H., Slomianny, C., Hakimi, M.A., Langsley, G., and Tomavo, S. (2016). A critical role for *Toxoplasma gondii* vacuolar protein sorting VPS9 in secretory organelle biogenesis and host infection. Sci. Rep. *6*, 38842.
47. Sheiner, L., Demerly, J.L., Poulsen, N., Beatty, W.L., Lucas, O., Behnke, M.S., White, M.W., and Striepen, B. (2011). A systematic screen to discover and analyze apicoplast proteins identifies a conserved and essential protein import factor. PLoS Pathog. *7*, e1002392.
48. Mirdita, M., Schütze, K., Moriwaki, Y., Heo, L., Ovchinnikov, S., and Steinegger, M. (2022). ColabFold: making protein folding accessible to all. Nat. Methods *19*, 679–682.
49. Callebaut, I., Labesse, G., Durand, P., Poupon, A., Canard, L., Chomilier, J., Henrissat, B., and Mornon, J.P. (1997). Deciphering protein sequence information through hydrophobic cluster analysis (HCA): current status and perspectives. Cell. Mol. Life Sci. *53*, 621–645.
50. Bruley, A., Bitard-Feildel, T., Callebaut, I., and Duprat, E. (2023). A sequence-based foldability score combined with AlphaFold2 predictions to disentangle the protein order/disorder continuum. Proteins *91*, 466–484.
51. Robert, X., and Gouet, P. (2014). Deciphering key features in protein structures with the new ENDscript server. Nucleic Acids Res. *42*, W320–W324.
52. Altschul, S.F., Madden, T.L., Schäffer, A.A., Zhang, J., Zhang, Z., Miller, W., and Lipman, D.J. (1997). Gapped BLAST and PSI-BLAST: a new generation of protein database search programs. Nucleic Acids Res. *25*, 3389–3402.
53. Zimmermann, L., Stephens, A., Nam, S.Z., Rau, D., Kübler, J., Lozajic, M., Gabler, F., Söding, J., Lupas, A.N., and Alva, V. (2018). A completely reimplemented MPI bioinformatics toolkit with a new HHpred server at its core. J. Mol. Biol. *430*, 2237–2243.
54. Pettersen, E.F., Goddard, T.D., Huang, C.C., Couch, G.S., Greenblatt, D.M., Meng, E.C., and Ferrin, T.E. (2004). UCSF Chimera-a visualization system for exploratory research and analysis. J. Comput. Chem. *25*, 1605–1612.
55. Holm, L. (2022). Dali server: structural unification of protein families. Nucleic Acids Res. *50*, W210–W215.
56. Sidik, S.M., Huet, D., Ganesan, S.M., Huynh, M.H., Wang, T., Nasamu, A.S., Thiru, P., Saeij, J.P.J., Carruthers, V.B., Niles, J.C., and Lourido, S.

(2016). A genome-wide CRISPR screen in *Toxoplasma* identifies essential Apicomplexan genes. Cell *166*, 1423–1435.e12.

57. Fauquenoy, S., Morelle, W., Hovasse, A., Bednarczyk, A., Slomianny, C., Schaeffer, C., Van Dorsselaer, A., and Tomavo, S. (2008). Proteomics and glycomics analyses of N-glycosylated structures involved in *Toxoplasma gondii*-host cell interactions. Mol. Cell. Proteomics *7*, 891–910.

58. UniProt Consortium (2021). UniProt: the universal protein knowledgebase in 2021. Nucleic Acids Res. *49*, D480–D489.

59. Jumper, J., Evans, R., Pritzel, A., Green, T., Figurnov, M., Ronneberger, O., Tunyasuvunakool, K., Bates, R., Žídek, A., Potapenko, A., et al. (2021). Highly accurate protein structure prediction with AlphaFold. Nature *596*, 583–589.

60. Varadi, M., Anyango, S., Deshpande, M., Nair, S., Natassia, C., Yordanova, G., Yuan, D., Stroe, O., Wood, G., Laydon, A., et al. (2022). AlphaFold protein structure database: massively expanding the structural coverage of protein-sequence space with high-accuracy models. Nucleic Acids Res. *50*, D439–D444.

STAR★METHODS

KEY RESOURCES TABLE

REAGENT or RESOURCE	SOURCE	IDENTIFIER
Antibodies (also see Table S3 for more details)		
Anti *Tg*REMIND	Tomavo Lab	In this study
Anti F-BAR	Tomavo Lab	In this study
Anti REMIND	Tomavo Lab	In this study
Anti *Tg*SORT	Tomavo Lab	Sloves et al.[22]
Rabbit Anti HA	Sigma	Cat#PLA 0001
Rat Anti HA	Roche Diagnostics	Cat#60789700
Anti Flag	Cell Signaling	Cat#2368
Anti cMyc	Thermo Fisher Scientific	Cat#13-2500
Anti GST	Thermo Fisher Scientific	Cat #MA4-004
Anti ROP1	Dubremetz Lab	N/A
Anti ROP4	Dubremetz Lab	N/A
Anti Pro ROP4	Gary Lab	N/A
Anti ROP5	Sibley Lab	Behnke et al.[12]
Anti ROP7	Dubremetz Lab	N/A
Anti GRA1	BIOTEM, France	Cat#BIO.018.4
Anti GRA2	BIOTEM, France	Cat#BIO.018.5
Anti GRA3	Dubremetz Lab	N/A
Anti GRA4	Dubremetz Lab	N/A
Anti GRA5	BIOTEM, France	Cat#BIO.018.6
Anti MIC2	Carruthers Lab	Harper et al.[16]
Anti MIC5	Carruthers Lab	N/A
Anti M2AP	Carruthers Lab	Harper et al.[16]
Anti proMIC5	Carruthers Lab	N/A
Anti MIC9	Soldati Favre Lab	Meissner et al.[8]
Anti VP1	Moreno Lab	N/A
Anti CPL	Moreno Lab	N/A
Anti HSP60	Tomavo Lab	N/A
Anti API (Trx)	Parsons Lab	N/A
CEN1	Gubbels Lab	N/A
IMC6	Bradley Lab	N/A
Anti SAG1	Dubremetz Lab	N/A
Goat anti rat Alexa Fluor 488 Antibody	Thermo Fisher Scientific	Cat#A11006
Goat anti mouse Alexa Fluor 568 Antibody	Thermo Fisher Scientific	Cat#A11004
Goat anti mouse Alexa Fluor 488 Antibody	Thermo Fisher Scientific	Cat#A322723
Goat anti rabbit Alexa Fluor 488 Antibody	Thermo Fisher Scientific	Cat#A11008
Goat anti rabbit 568 Alexa Fluor 568 Antibody	Thermo Fisher Scientific	Cat#A11011
Bacterial and virus strains		
NEB 5-alpha	Biolabs	Cat#C2987H
BL21-CodonPlus (DE3)	Biolabs	Cat#C2527H
Biological samples		
pLIC-cMyc-TUB5/CAT plasmid	Carruthers Lab	Huynh and Carruthers[27]
pG13-D-T7S4 plasmid	Striepen Lab	Sheiner et al.[47]
Rab5-HA plasmid	Meissner Lab	Kremer et al.[13]

(*Continued on next page*)

Continued

REAGENT or RESOURCE	SOURCE	IDENTIFIER
Rab7-HA plasmid	Meissner Lab	Kremer et al.[13]
HDEL-GFP plasmid	Meissner Lab	N/A
ERD-GFP plasmid	Meissner Lab	N/A
GalNac-T-GFP plasmid	Meissner Lab	N/A
DrpB-YFP plasmid	Meissner Lab	Breinich et al.[29]
Chemicals, peptides, and recombinant proteins		
Anhydrotetracycline (ATc)	Sigma-Aldrich	Cat#1035708
5'-Fluorodeoxyuridine (5'-FUDR)	Sigma-Aldrich	Cat#F0503
Pyrimethamine	Sigma-Aldrich	Cat#PHR3231
Chloramphenicol	Sigma-Aldrich	Cat#C0378
Isopropyl b-D-1-thiogalactopyranoside (IPTG)	Sigma-Aldrich	Cat#I5502
16% Paraformaldehyde	Thermo Fisher Scientific	Cat#28908
Freund's complete adjuvant	Thermo Fisher Scientific	Cat#77140
Freund's incomplete adjuvant	Thermo Fisher Scientific	Cat#77145
Dulbecco's modified Eagle medium–High Glucose	PAN Biotech	Cat#P04-03500
Bovine Serum (Calf Serum)	Dominique Dutscher	Cat#S1810
HisPur Ni-NTA chromatography cartridge	Thermo Fisher Scientific	Cat#90098
Glutathione Sepharose 4B column	GE healthcare	Cat#71024500
Anti HA-Agarose Beads	Thermo Fisher Scientific	Cat#26181
Anti cMyc-Agarose Beads	Pierce	Cat#20168
pGEX-full length TgREMIND	Genescript	In this study
pGEX-FBAR domain	Genescript	In this study
pGEX-REMIND domain	Genescript	In this study
HA-FBAR domain	Tomavo Lab	In this study
cMyc-REMIND domain	Tomavo Lab	In this study
Deposited data		
Mass spectrometry proteomics data generated by nanoLC-MS/MS analyses have been deposited to ProteomeXchange Consortium via PRIDE.	In this study	PXD025049 and https://doi.org/10.6019/PXD025049
3D structure model of the *Tg*REMIND F-BAR dimer (AlphaFold2)	In this study	https://doi.org/10.5281/zenodo.8002113
Experimental models: Cell lines		
Human Foreskin Fibroblast (HFF)	ATCC	HFF-1 ATCC SCRC-1041
Experimental models: Organisms/strains		
Toxoplasma. RH wild-type strain	Tomavo Lab	Sloves et al.[22]
Toxoplasma RHΔku80 strain	Carruthers Lab	Huynh and Carruthers[27]
Toxoplasma RHΔku80TaTi mutant	Striepen Lab	Sheiner et al.[47]
Toxoplasma iKO-TgSORT_HA mutant	Tomavo Lab	Sloves et al.[22]
Toxoplasma iKO-TgVps35_HA mutant	Tomavo Lab	Sangaré et al.[24]
Toxoplasma iKO-TgVps35_HA/KI-TgREMIND_cMyc line	Tomavo Lab	In this study
Toxoplasma iKO-TgREMIND-HA mutant	Tomavo Lab	In this study
Comp iKO-TgREMIND_HA/TgREMIND_Flag line	Tomavo Lab	In this study
Comp iKO-TgREMIND_HA/REMIND_Flag line	Tomavo Lab	In this study
Oligonucleotides		
The list of oligonucleotides sequence is shown in Table S1	N/A	N/A

(*Continued on next page*)

Continued

REAGENT or RESOURCE	SOURCE	IDENTIFIER
Recombinant DNA		
5'DNA TgREMIND-pG13-D-T7S4-DHFR-3'DNA TgREMIND	Tomavo Lab	In this study
5'UPRT-promTgREMIND-FLTgREMIND-3'SAG1-3' UPRT	Tomavo Lab	In this study
5'UPRT-promTgREMIND-FLTgREMIND-3'SAG1-3' UPRT	Tomavo Lab	In this study
5'UPRT-promTgREMIND-REMIND domain-3'SAG1-3' UPRT	Tomavo Lab	In this study
5'UPRT-promTgREMIND-FBAR domain-3'SAG1-3' UPRT	Tomavo Lab	In this study
pSAG1-CAS9-U6-sgUPRT	Addgene	Cat#54467
Software and algorithms		
FIJI (ImageJ)	https://fiji.sc	Version 2.0.0-rc-69/1.52i
GraphPad	https://www.graphpad.com	Version 9
Microsoft Excel	Microsoft.com	Version 2016
LibreOffice Calc	The Document Foundation https://www.libreoffice.org/	Version7,5,3,2
Microsoft Word	Microsoft.com	Version 2016
Inkscape	https://inkscape.org/fr/	Version 1.2.2
ColabFold v1.5.2	https://colab.research.google.com/github/sokrypton/ColabFold/blob/main/AlphaFold2.ipynb	Mirdita et al.[48]
DrawHCA	http://osbornite.impmc.upmc.fr/hca/hca-form.html	Callebaut et al.[49]
pyHCA	https://github.com/T-B-F/pyHCA	Bruley et al.[50]
ESPript 3.0	https://espript.ibcp.fr/ESPript/ESPript/	Robert and Gouet[51]
PSI-BLAST	https://blast.ncbi.nlm.nih.gov/	Altschul et al.[52]
HH-PRED	https://toolkit.tuebingen.mpg.de/#/tools/hhpred	Zimmermann[53]
Chimera	https://www.cgl.ucsf.edu/chimera/	Pettersen et al.[54]
Dali	http://ekhidna2.biocenter.helsinki.fi/dali/	Holm[55]

RESOURCE AVAILABILITY

Lead contact

Further information and requests for resources and reagents should be directed to and will be fulfilled by the lead contact Stanislas Tomavo: stanislas.tomavo@gmail.com or stanislas.tomavo@i2bc.paris-saclay.fr.

Materials availability

Plasmids and transgenic *T. gondii* mutants generated in this study will be shared by the lead contact upon request.

Data and code availability

- The mass spectrometry data were described in Table S1.
- The mass spectrometry proteomics data generated by nanoLC-MS/MS analyses have been deposited to the ProteomeXchange Consortium via PRIDE partner repository with the dataset identifier and accession code: PXD025049 and 10.6019/PXD025049.
- This paper does not report original code.
- Any additional information required to reanalyze the data reported in this paper is available from the lead contact upon request.

EXPERIMENTAL MODEL AND STUDY PARTICIPANT DETAILS

Growth of host cells and parasite strains

T. gondii RH wild-type strain, RHΔku80 (a strain with high homologous integration of transfected DNA[27]; and RHΔku80TaTi parasites, a Trans activator Trap identified inducible anhydrotetracycline (ATc) strain generated in the background of RHΔku80[48] were used. These parasites were maintained in monolayer human foreskin fibroblast (HFF) cultured in Dulbecco's Modified Eagle's Medium (DMEM) supplemented with 2 mM L-glutamine, 50 μg/mg penicillin/streptomycin and 10% fetal calf serum (FCS) (PAN Biotech, Dutscher, France) in a humid atmosphere under 5% CO_2 at 37°C as previously described[22].

Generation of *Tg*REMIND knockout and knock-in *T. gondii* strains

To obtain the conditional iKO-*Tg*REMIND in *T. gondii* RHΔku80-TaTi strain, we used the pyrimethamine-resistant plasmid pG13-D-T7S4 that contains the inducible promoter TeTO7-Sag4. We first amplified by PCR 2 kb of 5'-DNA fragment of *Tg*REMIND, which was cloned into NdeI restriction enzyme site. After verification of the correct orientation using StuI/EcoRV, we cloned the 1.3 kb 3'-DNA TgREMIND fragment containing an epitope HA downstream of the inducible promoter. All oligonucleotides used during this work were listed in Table S2 (see Supplemental Information). Fifty μg of this plasmid was linearized with EcoRV and used to transfect 10^7 tachyzoites of RHΔku80-TaTi that were selected with 2 μM of pyrimethamine before cloning by limiting dilution to obtain the conditional iKO-HA-*Tg*REMIND mutants. We used the pUPRT (Uracil PhosphoRibosyl Transferase) plasmid to complement these mutants, in which either 2 kb of TgREMIND, 1 kb of Tubulin, or 1.5 kb of GRA1 promoter was respectively cloned downstream of the 5'UPRT using AscI/StuI. Then, the entire length of *Tg*REMIND (2928bp) was tagged to the epitope FLAG using StuI/AvrII. Finally, the 3'SAG1 untranslated region (350bp) was cloned upstream of the 3'UPRT region using AvrII/PacI. This later plasmid was used for subcloning and replacing the DNA coding full-length TgREMIND by the 1.15 kb or 1.77 kb of DNA coding, respectively, the N-terminus F-BAR and C-terminus REMIND domains with all tagged to the epitope FLAG using StuI/AvrII. DNA sequencing (Genewiz, Germany) using primers listed in Table S2 checked the accuracy of all plasmids. After co-transfection of 10^7 iKO-HA-*Tg*REMIND parasites of those above linearized, 50 μg of each linearized plasmid to which 10 μg of pSAG1::CAS9-U6::sgUPRT was added to favor a high rate of homologous recombination into UPRT locus[56]. Twenty hours later, the co-transfected parasites were incubated with 5μM of 5-fluoro-2'-deoxyuridine (5' FUDR), and the stable parasite lines obtained were cloned by limiting dilution. After screening by indirect immunofluorescence assays (IFA) using anti-HA or anti-FLAG, the positive clones were selected. The iKO-TgVps35-HA/KI-TgREMIND-cMyc line was generated using the iKO-TgVps35-HA[24] and pLic-cMyc-TUB5/CAT plasmid[27] containing 3 kb genomic DNA of TGGT1_259720 gene upstream to stop codon. After linearization of the plasmid by BstZ171, $5x10^6$ parasites were transfected with 50 μg of plasmid, and the stable line was selected with 20 μg of chloramphenicol.

METHOD DETAILS

Immunofluorescence assays

Paraformadehyde-fixed intracellular parental RHΔku80-TaTi and iKO HA-*Tg*REMIND mutants treated or not with 1.5 μg/ml of anhydrotetracycline (ATc) were used for immunofluorescence assays. The list of monoclonal and polyclonal antibodies used and their dilutions are listed in Table S3 (Supplemental Information). Alexa Fluor secondary antibodies (488 nm, 568 nm, 594 nm) from either rat, rabbit, or mouse were chosen depending on the nature of primary antibodies used at 1:1000 dilutions. In some cases, when a specific primary antibody was not available, we transiently transfected $5x10^6$ tachyzoites with plasmids expressing different markers of subcellular compartments such as ELC (Rab5-HA and Rab7-HA), endoplasmic reticulum (HDEL-GFP), ER/post-Golgi (ERD-GFP), post-Golgi (GalNac-T-GFP) and dynamin-containing compartment (DrpB-YFP[29]).The antibodies specific to HA or anti-GFP were used to amplify the fluorescence, then anti-TgREMIND and mouse secondary antibodies were used for co-distribution studies.

Confocal laser scanning microscopy

The acquisition of fluorescence images was performed using the Leica SP8-X (Leica DMI 6000) microscope with a 63x objective. ImageJ was used for image processing, and Pearson's coefficient for quantification from 4 to 6 vacuoles, each containing between 4 to 16 parasites. The primary antibodies and dilutions used are listed in Table S3. The secondary antibodies used were either goat anti-mouse, anti-rat, or anti-rabbit conjugated to Alexa Fluor 488, 568, or 594 nm (Invitrogen or Thermo Fisher Scientific, France).

Confocal spinning disc microscopy

IFA images were also obtained using the Inverted Nikon Ti Eclipse Eclipse-E microscope coupled with a spinning disk (Yokogawa, CSU-X1-A1), a 100x plan apo objective (Nikon, NA 1.49, oil immersion), and an sCMOS camera (Photometrics, Prime 95B). An additional "Live-SR" module (GATACA systems) was added to increase two fold the resolution. DAPI fluorescence was detected after a 405 nm excitation (Vortran, 100 mW laser) with a 450/50 bandpass filter (Chroma). Alexa 488 was detected after a 488nm excitation (Vortran, 150mW laser) with a 524/45 bandpass filter (Semrock). Alexa 568 was detected after a 561nm excitation (Coherent, 100mW laser) with a 607/36 bandpass filter (Semrock). The whole system was driven by Metamorph (version 7.7, Molecular Devices).

Electron and immunoelectron microscopy

Intracellular parasites were fixed at room temperature for 1h in 0.1 M sodium cacodylate buffer containing 2.5% glutaraldehyde. Then, samples were kept overnight at 4°C. After washing with the same buffer, samples were fixed again in aqueous 1% osmium tetroxide and 1.5% potassium ferrocyanide. After successive dehydration in ethanol, samples were embedded in Epon (Agar Scientific, AGR1165): 2h in resin mixed with ethanol and 2h with pure resin before polymerization 24h at 60°C. Sections of 70 nm were cut using an ultramicrotome LEICA UC6, collected on grids, and contrasted 15min in 2% aqueous uranyl acetate and 2min in Reynold's lead citrate. Ultrastructural images were collected using a JEOL1400 transmission electron microscope at 80kV and camera RIO9. For immuno-electron microscopy, the HFF cells infected with iKO-TgREMIND mutants treated with ATc for 36 hours or untreated were fixed overnight at 4°C in 8% paraformaldehyde with 0.1% glutaraldehyde in PBS buffer, thoroughly washed in the same buffer, pelleted in 10% gelatin and infused overnight in sucrose 2.3 M containing 20% polyvinyl pyrrolidone 10000 in phosphate buffer 0.1 M. The pellets were mounted on ultracryomicrotome supports and rapidly frozen in liquid nitrogen. Ultrathin sections of about 90–100 nm were obtained using a UC6 ultramicrotome equipped with an FC6 device (Leica). For immuno-labeling, sections were incubated in blocking medium (0.05 M glycine, 5% fish gelatine in 0.1 M PBS buffer) for 30 min. The grids were incubated with rabbit polyclonal anti-ROP1 or monoclonal anti-GRA1 antibodies for 1.5 hour at 37°C. After washing, sections were incubated at room temperature for 30 min in the corresponding secondary gold conjugates (Aurion, 10nm gold-labeled antibody) diluted in the same buffer. Following a final thorough wash in PBS alone, the grids were fixed in 4% glutaraldehyde for 10 min at room temperature and washed in water. After staining 0.5% uranyl acetate in 1.5% methylcellulose, sections were observed on a JEOL1400 transmission electron microscope at 80 kV accelerating voltage.

Production of glutathione-*S*-transferase (GST) recombinant proteins and specific antibodies

The full length of *Tg*REMIND DNA sequence and those of its N-terminus F-BAR and C-terminus REMIND domains were synthesized and cloned into the pGEX plasmid by GenScript using the restriction enzymes BamHI and NcoI. BL21 DE3 *Escherichia coli* (Biolabs) was used to transform and produce recombinant proteins. First, pre-cultures of 10 ml grown in the presence of ampicillin (100 μg/ml) at 37°C overnight were transferred to one-liter cultures, which were incubated at 37°C for 4 to 5 hours to reach OD_{600} of 0.6. Production of these recombinant proteins was induced with 0.2 mM isopropyl β-D-1-thiogalactopyranoside (IPTG) at 20°C overnight and checked by SDS-PAGE. Next, cultures were centrifuged at 6000xg at 4°C for 15 min. Pellets were frozen at -80°C for at least 2 h before lysis in 50 mM Tris-HCl pH 8 buffer, 250 mM NaCl, 5% glycerol, and 0.1% Triton X-100 supplemented with 1X protease inhibitors, 1 mg/ml lysozyme, 5 mM DTT and 1 mM Phenylmethylsulfonyl fluoride (PMSF). After incubation for 30 min on ice, bacteria were lysed by 6 cycles of sonication (30 s pulse at 90% and 20 s pause) and centrifuged at 2000 rpm and 4°C. Next, the supernatants were incubated with a GST column overnight at 4°C with 5 mM ATP and 1 mM PMSF. Two washes were performed at pH 7.5 with two different washing buffers: 50 mM Tris-HCl, 1 M NaCl, 5 mM DTT, and 50 mM Tris-HCl, 150 mM NaCl, and 5 mM DTT. Finally, recombinant proteins were eluted for 10 min at 4°C using 50 mM Tris-HCl pH 8, 150 mM NaCl, 10 mM GSH (glutathione), 5 mM DTT, and 0.5 mM PMSF buffer. The eluates were dialyzed and concentrated by the Amicon system before SDS-PAGE and Coomassie blue staining. The purified recombinant full-length GST-FL_TgREMIND, GST_F-BAR, and GST_REMIND proteins were used to immunize a group of five Balb/c mice using 50 μg of protein (per mouse) and complete Freund adjuvant. The mice were challenged three times with the same amount of protein prepared in incomplete Freund adjuvant. After a last boost, the sera were collected and tested by Western blots and IFA. The positive sera specific to each recombinant protein were pooled and purified.

Lipid overlay experiments

The phosphatidylinositol lipids (Avanti polar lipids) were resuspended with a 2:1:0.8 (Methanol: Chloroform: Water) ratio at a final concentration of 2pmol/μL. One μl of each lipid was spotted on nitrocellulose Hybond extra membrane (GE Healthcare), then dried at room temperature for 1 hour. The lipid-spotted membranes were then saturated at room temperature for an hour with a buffer 50mM Tris-HCl, pH 7.5, 150mM NaCl, 0.1% ovalbumin, and 0.01% Tween 20. The lipid-spotted membranes were incubated overnight à 4°C in the same buffer with 0.2 to 5 μg of freshly purified GST-TgREMIND, GST-F-BAR, GST-REMIND, and GST as a negative. The recombinant proteins tagged to a smaller tag, such as HA and cMyc, were also produced, purified from *E. coli*, and tested. The lipid-spotted membranes were washed with TBST buffer (Tris-Buffered Saline Tween) and revealed using (species) anti-GST diluted at 1:1000 (Thermo Fisher Scientific), and secondary antibody HRP at 1:5000 was added. The blots were revealed with ECL after washings with the same buffer (Enhanced ChemiLuminescence Detection System, Amersham Biosciences). All blots were scanned at identical time exposure of 500 s.

GST pull down and liquid chromatography-tandem mass spectrometry

To identify *Tg*REMIND partners, 10^9 tachyzoites of RH strain were lysed for 1 h at 4°C under rotary shaking in a buffer containing 10 mM Tris-HCl, 150 mM NaCl, 1 mM $MnCl_2$, 1 mM $CaCl_2$, 1% Triton X-100 and protease inhibitors. The lysate was centrifuged at 10,000 rpm for 30 minutes at 4°C, and supernatants were incubated with 100 μg of each recombinant protein GST-*Tg*REMIND, GST-F-BAR, GST-REMIND coupled to GST beads or with GST alone (negative control) at 4°C overnight. Five washings were performed with lysis buffer before elution. Sixteen μl of eluates were mixed with 4 μl of 5X Laemmli buffer and heated at 100°C for five minutes. SDS-PAGE was performed using 12% polyacrylamide gel under reducing conditions at 30 V for staking, then at

70 V and 120 V for separation. Gels were then stained with BIO-RAD Coomassie brilliant blue R-250. As described below, the protein bands of interest were excised and processed for mass spectrometry analysis.

In-gel digestion of protein and LC-MS/MS analysis

Gel bands corresponding to each eluate from the pull-down using GST-TgREMIND, GST-F-BAR, and GST-REMIND were processed for in-gel digestion following the Thermo-Fisher protocol. The resulting peptide samples were separated using the Ultimate 3,000 RSLC nano- System (Dionex, Thermo Scientific) connected to a Q-HF orbitrap mass spectrometer. A nano column (Acclaim PepMap RSLC, 15 cm × 75 μm inner diameter, C18, 2 μm, 100 Å; Dionex, Sunnyvale, CA). The elution was done by applying a mixture of solvent A (HPLC grade water with 0.1% formic acid). Solvent B (HPLC grade acetonitrile with 0.1% formic acid) at the flow rate of 300 nL per min by applying a linear gradient from 2 to 40% solvent B over 38 min followed by a washing step for 5 min with70% solvent B and an equilibration step for 11 min with 2% solvent B. A nanospray Flex Ion Source was used for ionization with a voltage set at 1.9 kV and a capillary temperature of 275 °C. Full MS scans were acquired in the Orbitrap mass analyzer over an *m/z* range of 300-3,500 and a resolution of 70,000 at *m/z* 200. The target automatic gain control value of 1×10^6 was used with a maximum allowed injection time (Maximum IT) of 250 ms. For MS/MS, an isolation window of 2 *m/z* was utilized. Peptide fragmentation was performed using high-energy collision-induced dissociation with a normalized collision energy set at 35. The tandem mass spectra were acquired over the *m/z* 200-2,000 range in the Orbitrap mass analyzer with a resolution of 35,000 at *m/z* 200 and automatic gain control of 2×10^5. The ion intensity selection threshold was 6.7×10^4, and the maximum injection time was 150 ms. All these systems were entirely controlled by Thermo Xcalibur 3.0 (Thermo Fisher Scientific). All collected data files (*.raw) were processed with a specific workflow designed in Proteome Discoverer 1.4 (Thermo Fisher Scientific). MS/MS data was interpreted using two search engines, Mascot (version 2.4.1, Matrix Science, London, UK) and Sequest HT (Thermo Fisher Scientific). Searches were performed against *T. gondii* (TGVEG, TGME49, and TGGT1 strains) protein sequences downloaded from www.toxodb.org.[57] The Mascot ion score was >20, and Sequest HT XCorr >1.5. The decoy database search allowed us to control and estimate the false positive identification rate.

Cell fractionation

Extracellular parasites that were freshly egressed of wild-type *T. gondii* RHΔku80 (10^8 tachyzoites) were purified to remove HFF debris, pelleted, and washed once with PBS as described[29]. Each pellet was resuspended with 300 μl of each different lysis buffer as follows: PBS 1x, 2% Triton X-100 in 1x PBS, 1M NaCl in 1x PBS, and 0.1 M Na_2CO_3 in PBS 1x at pH 11.5. After lysis by three series of rapid freezing in liquid nitrogen and thawing in a water bath at 37°C, sonication obtained homogenates. The different homogenates underwent ultracentrifugation at 100,000xg at 4°C to separate into different soluble and insoluble fractions. Fractions equivalent to $1x10^7$ parasites were analyzed by SDS-PAGE followed by immunoblots using specific anti-TgREMIND, anti-Glycosyl Phosphoribosyl Inositol (GPI) anchored SAG3 and anti-G6-PI (glucose 6-phosphate isomerase) antibodies.

Microneme secretion and dense granule excretion

Freshly egressed ($2x10^8$ parasites) ATc-treated (1.5 μg/ml) or untreated iKO-TgREMIND mutants for 48 h were harvested by centrifugation at 600 x g for 10 min at room temperature. The samples were washed twice with prewarmed at 37°C of intracellular buffer containing 5 mM NaCl, 142 mM KCl, 1 mM $MgCl_2$, 2 mM EGTA, 5.6 mM glucose and 25 mM HEPES, pH 7.2). After centrifugation, parasites were resuspended in DMEM supplemented with 2 mM glutamine containing 500 μM of propranolol or not and incubated for 20 min at 37 °C (Bullen et al., 2016). Parasites were centrifuged at 1000 × g, 4 °C for 5 min. Pellets were washed once in PBS and resuspended in Laemmli buffer. Supernatants were centrifuged at 2000 × *g* for 5 min, 4 °C, and supernatants used as ESA (Excreted/Secreted Antigen) were also suspended in 2XLaemmli buffer. Pellets and ESA samples were run on SDS-PAGE and analyzed for the presence of dense granule GRA1 and microneme MIC9 by Western blots.

Co-immunoprecipitations, SDS-PAGE and western blots

For co-immunoprecipitations, $2x10^8$ parasites from transgenic knocked in of cMyc-TgVps35 into iKO-TgSORT mutants freshly egressed after ATc-treatment or not for 48h were purified and extracted with Triton X-100 as described (Fauquenoy et al., 2011). Binding protein complexes of co-immunoprecipitation or total protein extracts of purified parasites were electrophoresed on SDS-PAGE, transferred at 80 V for 1 h 15 min onto a nitrocellulose membrane in a cold buffer containing 25 mM Tris-HCl, 190 mM glycine and 20% methanol in a cold room. After 5 min of 0.2% Ponceau red staining, water-rinsed membranes were saturated with 5% skim milk prepared in TNT buffer (15 mM Tris-HCl pH 8; 140 mM NaCl; 0.05% Tween-20) for 30 min at room temperature. The primary antibodies used are listed in Table S3. The secondary peroxidase-coupled antibodies (Sigma, France) or Alexa fluor 647 nm (Invitrogen, France) or Plus 800 nm (Thermo Fisher Scientific) antibodies (Invitrogen, France) prepared in TNT were incubated for 1 h at room temperature. Following three washes, the blots were revealed with ECL (Enhanced ChemiLuminescence Plus Western Blotting Detection System, Amersham Biosciences) whereas the Alexa fluor antibodies were directly scanned using VILBER Fusion FX imaging apparatus (France).

Gliding assay and host cell invasion

Trail deposition assays were performed as previously described.[58] ATc-treated iKO-TgREMIND and ATc-treated complemented Comp-KO-TgREMIND parasites for 48h were purified, and pellets were resuspended with incomplete DMEM medium supplemented

with 10 mM HEPES and 1 mM EGTA. Parasites (5.10^6 tachyzoites) were plated on glass coverslips previously treated with 50% FCS at 37°C overnight. After 20 minutes of incubation at 37°C under 5% CO_2, parasites were fixed with 4% PFA. Gliding trails were observed under a Zeiss fluorescence microscope after staining with SAG1 antibodies. For host cell invasion, iKO-TgREMIND, Comp-full length TgREMIND_FLAG and Comp-REMIND_FLAG were treated or not with ATc for 48h. Freshly egressed parasites were used to infect confluent HFF cells and processed as described[24].

Plaque assays

Plaque assays were carried out as previously described[22], except that the coverslip containing confluent HFF cells were infected with 500 iKO-*Tg*REMIND, Comp-iKO*Tg*REMIND, Comp-REMIND, and RHTaTi. After 3h post-infection, 1.5 μg/ml of ATc was added or not to these infected HFF coverslips and incubated for seven days. Infected HFF cells were fixed with cold methanol on ice for 10 min before staining with crystal violet at room temperature for 10 min. After three washes with distilled water, the coverslips were air-dried before imaging.

Bioinformatics analyses

Sequences were downloaded from the UniProt database[59] or from the *Toxoplasma* genome database (www.toxodb.org). Hydrophobic Cluster Analysis (HCA) plots of the *T. gondii* hypothetical proteins were drawn using DrawHCA (http://osbornite.impmc.upmc.fr/hca/hca-form.html). In this duplicated two-dimensional representation of the protein sequence, strong hydrophobic amino acids (V, I, L, F, M, Y, W) are contoured, forming clusters, which have been shown to mainly correspond to regular secondary structures[49]. Regions with high density in hydrophobic clusters form foldable domains, which can be automatically delineated using SEG-HCA[49]Jumper, now included in the pyHCA package[50]. AlphaFold2 (AF2)[59] models were extracted from the AFDB database[60]. The model of the TgREMIND F-BAR/REMIND dimer (aa 80-830) was made using ColabFold v1.5.2[48]. Sequence similarities were initially searched against UniProt using PSI-BLAST[52]. HH-PRED[53] was used to search protein domain and structure databases. A comparison of 3D structures against those included in the Protein Data Bank (PDB) was performed using DALI[55]. 3D structures were visualized with the UCSF Chimera package[54]. Sequence alignment was rendered using ESPript[52].

QUANTIFICATION AND STATISTICAL ANALYSIS

All statistical analyses were performed using GraphPad Prism 9 and LibreOffice Calc. Unless otherwise noted, all error bars are presented as the standard deviation (SD) and from a minimum of three independent trials. Significant differences were only considered if P values were < 0.05, where *$p < 0.05$; **$p < 0.01$; ***$p < 0.001$; and ****$p < 0.0001$. NS designates when the comparison is not statistically significant. Statistical studies were performed using ANOVA one-way or two-way followed by Tukey's multiple comparisons tests.